CrossMark

REVIEW

Beyond Graphene Anode Materials for Emerging Metal Ion Batteries and Supercapacitors
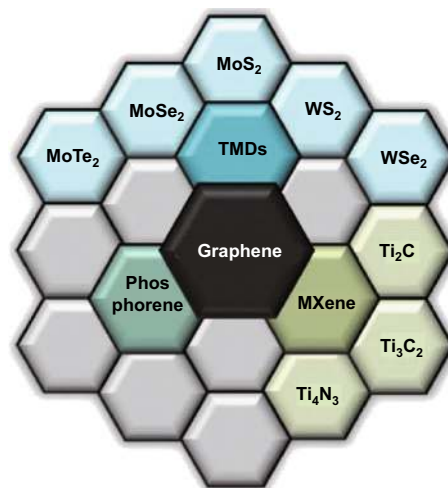
Santanu Mukherjee[1] · Zhongkan Ren[1] · Gurpreet Singh[1]

© The Author(s) 2018

Highlights

- A comprehensive review of novel 2D materials, particularly MXene and phosphorene, for applications as electrodes in both batteries and supercapacitors. The performance of these materials, in addition to their fabrication techniques, structure, and electrochemistry, is highlighted.
- Separate sections are dedicated to explaining the limitations of conventional anode materials and the role of 2D materials in addressing these deficiencies, in addition to the future path of development of this field of research.

Abstract Intensive research effort is currently focused on the development of efficient, reliable, and environmentally safe electrochemical energy storage systems due to the ever-increasing global energy storage demand. Li ion battery systems have been used as the primary energy storage device over the last three decades. However, low abundance and uneven distribution of lithium and cobalt in the earth crust and the associated cost of these materials, have resulted in a concerted effort to develop beyond lithium electrochemical storage systems. In the case of non-Li ion rechargeable systems, the development of electrode materials is a significant challenge, considering the larger ionic size of the metal-ions and slower kinetics. Two-dimensional (2D) materials, such as graphene, transition metal dichalcogenides, MXenes and phosphorene, have garnered significant attention recently due to their multi-faceted

Santanu Mukherjee and Zhongkan Ren have contributed equally to this work.

✉ Santanu Mukherjee
santanum@ksu.edu

✉ Gurpreet Singh
gurpreet@ksu.edu

1 Department of Mechanical and Nuclear Engineering, Kansas State University, Manhattan, KS 66506, USA

advantageous properties: large surface areas, high electrical and thermal conductivity, mechanical strength, etc. Consequently, the study of 2D materials as negative electrodes is of notable importance as emerging non-Li battery systems continue to generate increasing attention. Among these interesting materials, graphene has already been extensively studied and reviewed, hence this report focuses on 2D materials beyond graphene for emerging non-Li systems. We provide a comparative analysis of 2D material

chemistry, structure, and performance parameters as anode materials in rechargeable batteries and supercapacitors.

1 Introduction

LIBs have been the predominant rechargeable metal ion battery system for energy storage ever since they were first introduced commercially by Sony in the early 1990s [1]. They have become ubiquitous in their applications, which include smartphones and tablets, and even battery-powered vehicles [2, 3]. It is not an exaggeration to suggest that LIBs have played a leading role in revolutionizing the field of consumer electronics. There are several reasons for the excellent performance of LIBs; the relatively small ionic size of Li^+ (0.76 Å) and the consequent ease of intercalation into host lattices, the large energy and power densities and the low reduction potential ($-$ 3.04 V vs standard hydrogen electrode) [4, 5] are a few examples. Regardless of these advantages, LIBs are hindered by several important deficiencies. The elevated reactivity of Li metal, the flammability of organic electrolytes, the low quantity of raw material (Li) in the earth's crust leading to a high cost of Li procurement and other issues related to the disposal of spent cells are some of the major concerns that are posed by current LIB systems [1, 6].

With this perspective in mind, there has been a dedicated effort to develop viable alternatives to LIBs in recent years. A few examples of notable non-LIB metal ion rechargeable battery systems that have received significant attention include the sodium ion battery system (SIB), the potassium ion battery system (KIB), the magnesium ion battery system (MIB) along with aluminum and calcium ion battery systems [7, 8]. These materials are significantly more abundant in the earth's crust than Li, and their disposal does not pose as much of an environmental hazard. Consequently, they are being proposed for applications in medium- to large-scale grid storage systems [5, 9]. However, the large size of these ions (Na^+, K^+ etc.) often results in challenges during intercalation, lower ionic mobilities, and poor kinetics [4, 10]. For example, Na^+ ion cannot intercalate easily into graphite (the standard anode material for LIB systems) due to its large size and energetic considerations [11]. Therefore, the careful reconfiguration of the microstructure and efficacious engineering of the electrode design is of considerable significance. Table 1 provides a co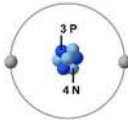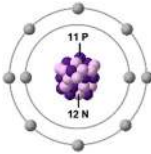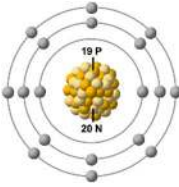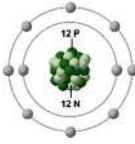mparative analysis of the important aspects associated with the different types of metal ions for emerging rechargeable electrochemical storage devices with respect to lithium.

A schematic representation of the different types of conventional electrochemical energy storage systems, the economics involved, and their performance criteria are provided in Fig. 1. It is noted that LIBs provide significantly low self-discharge characteristics and high efficiency compared to other electrochemical energy storage systems. Therefore, to match the best performance of LIBs and to improve upon those aspects where they are inferior, the development and understanding of novel anode materials is necessary. Hence, novel 2D materials are investigated. Based on their properties, it is expected that 2D materials will be able to enhance the performance of non-Li metal ion rechargeable batteries.

2D materials have recently received widespread attention, especially for applications in electronic devices, electrochemical energy storage (batteries and supercapacitors), anti-corrosion applications, photonics, etc. [5]. These materials present layered structures with a dimensional constraint in one direction [5, 13]. This layered structure provides a large surface area which makes them attractive for applications as negative electrodes in electrochemical energy storage systems [13].

Graphene is a single sheet of graphite and is one of the most popular 2D materials [13, 14]. The popularity of this material stems from its diverse range of favorable properties; large intrinsic carrier mobility [$\sim$ 200,000 cm^2 (Vs)$^{-1}$], high mechanical strength (Young's modulus of $\sim$ 1 TPa), very high electrical conductivity ($\sim$ 106 S cm^{-1}), and high theoretical specific surface area (2630 m^2 g^{-1}), as examples [15–17]. A large number of diverse studies have been performed on graphene with an emphasis on potential applications ranging from electrochemistry to solar cells, based on these superior properties [14, 18]. *Transition metal dichalcogenides* (TMDs), e.g., MoS_2, $MoSe_2$, WS_2, WSe_2, are a class of compounds with layered structures that have demonstrated promise for electrochemical energy storage and other applications including as catalysis, sensors, piezoelectric devices [19, 20]. *MXenes* are 2D inorganic compounds (usually transition metal nitrides or carbides) that continue to generate considerable interest [21]. They possess good conductivity and are being investigated as anodes for battery and supercapacitor applications as well as for other areas such as hydrogen storage and as adsorbents [22, 23]. *Phosphorene* is single layer/few layers of black phosphorus (BP), which is regarded as another novel 2D material with interesting properties [24]. Phosphorene possesses a hexagonal lattice structure which resembles graphene and has been targeted for applications in electrochemical energy storage, solar cells, sensors, etc. [25–28]. Figure 2

Table 1 Comparison of the critical parameters of Li with other important metal ions that are used in emerging metal ion rechargeable electrochemical storage devices. These parameters play an important role in determining the choice of raw material

Important parameters	Li$^+$	Na$^+$	K$^+$	Mg^{2+}	Ca^{2+}	References
Ionic structure						
Ionic (Shannon) radii (Å)	0.76	1.02	1.38	0.72	1.00	[4]
Relative atomic mass	6.94	23.00	39.10	24.31	40.07	[5]
Abundance in earth crust (wt%)	0.0017	2.6	2.4	1.9	3.4	[5, 9]
Atomic density (g cm^{-3})	0.534	0.968	0.89	1.738	1.55	*
E_0 versus SHE (V)	− 3.04	− 2.71	− 2.93	− 2.70	− 3.80	[5]
Theoretical capacity						
(mAh g^{-1})	3861	1166	685	2205	1340	[5, 9]
(mAh cm^{-3})	1378	1193	1059	1085	987	[5]
Cost of industrial grade metal (US$/ton)	130,000	3200	14,000	2300	3300	**

*J.A. Dean (ed), Lange's Handbook of Chemistry (15th Edition), McGraw-Hill, 1999; Section 3; Table 3.2 Physical constants of inorganic compounds

**http://original.metal.com
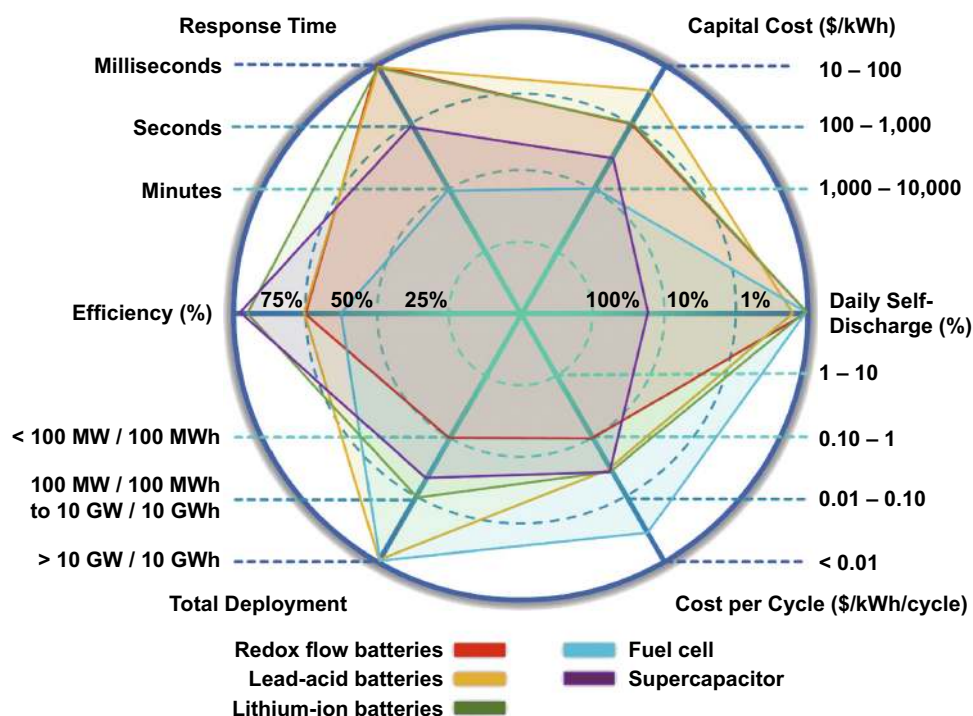
Fig. 1 Spider graph representation of critical parameters of the different electrochemical energy storage systems. Data for the figure have been obtained from Ref. [12]

illustrates a detailed diagrammatic representation including a statistical analysis of the different areas of application of 2D-layered materials beyond graphene.

A large number of reports on the application of graphene as an electrode material for electrochemical energy storage devices already exist in the scientific literature [29, 30]. Therefore, as a forward-looking review, this article will

focus on the analysis and review of 2D materials beyond graphene in emerging non-Li rechargeable electrochemical energy storage systems.

2 Current State-of-the-art and 2D Materials as Anodes for Emerging Metal Ion Rechargeable Battery Systems

The current state-of-the-art anodes for non-Li rechargeable metal ion battery systems consist of a diverse class of compounds. The subsequent paragraph will provide a brief discussion of these compounds and detail how 2D materials can be used to address their deficiencies.

Initially, different carbonaceous materials, e.g., graphite, hard carbons, were considered for application as anodes. However, the storage of Na^+ ions in graphite is unsuitable due to the lack of sufficient host sites and the unfavorable energetics, and the storage capacity of sodium in graphite is consequently only 35 mAh g^{-1} [9]. Potassium intercalates into graphite unlike sodium; however, large voltage hysteresis is prevalent and the rate capabilities are relatively poor at high C rates [31].

Metal oxides are another important class of compounds that have been investigated for this purpose. Oxides such as Fe_2O_3, CuO have a high theoretical storage capacity for sodium. However, they undergo large volume changes due to a conversion reaction which reduces their lifespan and thereby limits their utility in this regard [9]. NASICON-type anodes, e.g., $NaTi_2(PO_4)_3$, provide a potential solution to this problem with their high structural stability and good ionic conductivity [32]. However, they exhibit poor electronic conductivities and are relegated to being used primarily as composites [32]. Composite metal oxides such as Co_3O_4–Fe_2O_3 have shown some promise in KIB systems with demonstrated capacities of 350 mAh g^{-1} [33]. Low-strain transition metal oxides such as $Li_4Ti_5O_{12}$ for MIB systems have also been investigated and have demonstrated good cycling abilities, but a more thorough evaluation is necessary [34].

Alloy-based anodes (alloys of Sn, Sb, etc.) have been investigated as potential anodes for SIB systems. In particular, Sn-based alloys provide a theoretical capacity as high as 790 mAh g^{-1}. However, the potential application of these alloys is restricted due to their large volume expansion ($\sim$ 520% for some Sn alloys) as a result of the
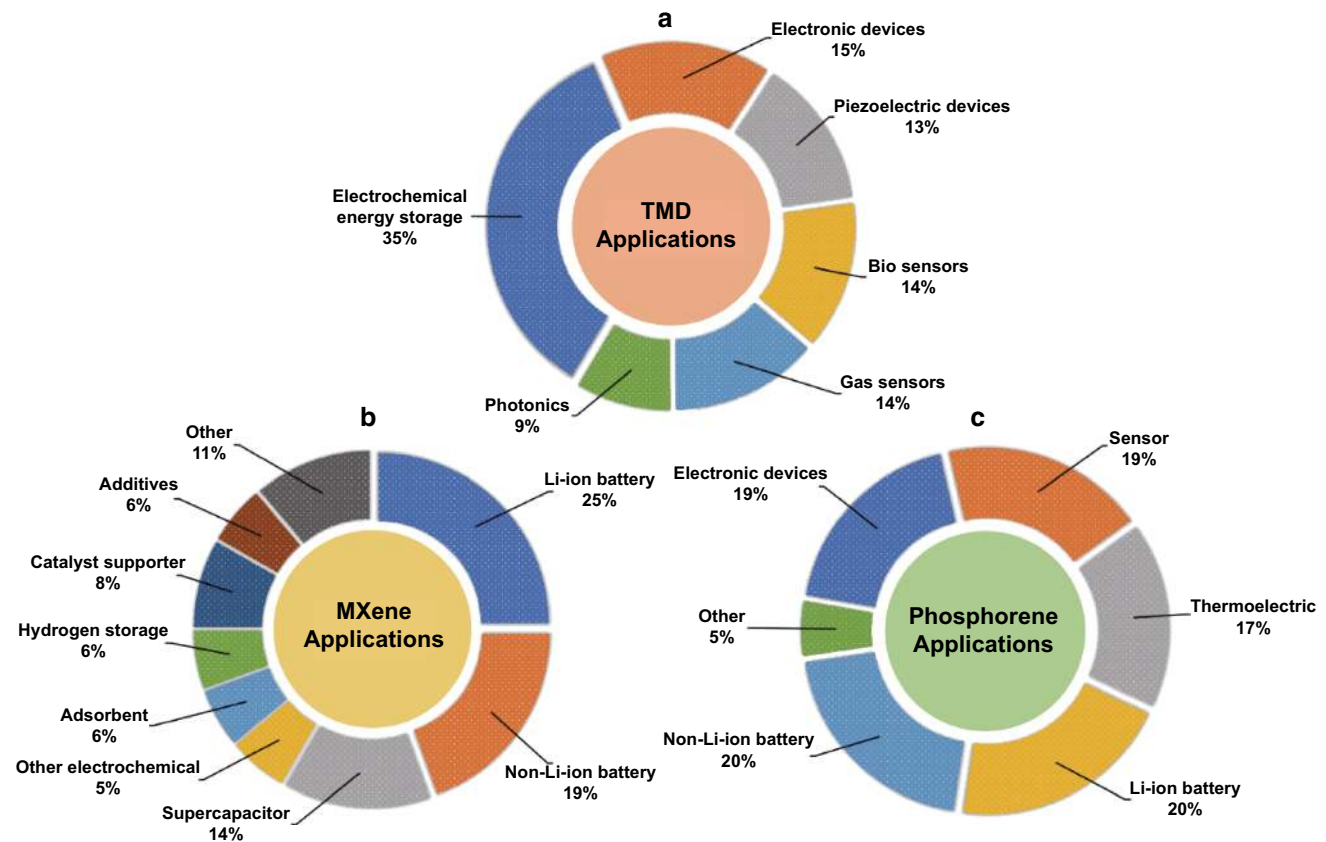
Fig. 2 Statistical analysis of the application of beyond graphene 2D materials: **a–c** Pie chart analysis showing the weight of the various applications of TMDs, MXene, and phosphorene, respectively. Electrochemical energy storage occupies an important role in the application regimes of each of the 2-D materials, which is indicative of the current trend of their applications in batteries and supercapacitors

alloying/intercalation process. As a result, stability issues are often encountered [35]. Phosphorus has been used as an alloying anode material for KIB systems because of its large theoretical capacity (843 mAh g^{-1}). However, the issue of large volume expansion ($\sim$ 190%) is also prevalent and causes rapid capacity fading [36]. Metal alloys, e.g., Bi-Sb, have also been investigated as anodes in MIB systems because of their high theoretical capacity ($\sim$ 2205 mAh g^{-1}). However, in this case, the problem lies in developing a better understanding of the electrode–electrolyte interface because conventional anodes are unsuitable in the electrolyte of choice [37].

2D materials with their unique properties are well suited to overcome the limitations of conventional anode systems. These materials can be fabricated with relative ease by liquid-based exfoliation techniques with a high degree of scalability [13]. Because the exfoliation process does not typically involve any chemical reactions, the resulting 2D materials are able to retain their morphology and chemical structure [13]. These materials have a large surface area due to their morphology, enhanced kinetics and high theoretical capacities. One of the most important aspects of 2D materials is that their interlayer spacing can be manipulated by pre-intercalating guest species (e.g., metal ions, polymers etc.) inside their layers during the fabrication process [38, 39]. For example, in TMDs, the rather large interlayer spacing (e.g., 0.65 nm for MoS_2) provides a rather conducive environment for accommodating large-sized alkali metal ions such as Na^+, K^+ [5]. MXene layers/sheets have also demonstrated excellent electrical conductivity and efficient sodium storage capacity [5]. Phosphorene has also demonstrated high theoretical capacities and is more stable unlike its bulk precursor, black phosphorus, which undergoes large volume changes during interaction with intercalating ions [40].

3 Structure and Electronic Properties of 2D Materials

The crystal structure and electronic properties of 2D materials are important aspects that determine their overall electrochemical performance and therefore merit a detailed overview. Also, the properties of these materials in their single-/few-layered forms are different from those of their bulk morphology. This aspect plays an important role in influencing their performance as electrodes [41]. The following subsections discuss these properties in greater detail.

3.1 TMDs

TMDs usually demonstrate the empirical chemical formula given by MX_2, where M is a transition metal (Mo, W etc.) and X is a chalcogen atom (S, Se, etc.) [42]. Consequently, a wide variety of TMDs exists with different fundamental properties: from the semiconducting MoS_2 to the semi-metal WTe_2 [41, 43]. The TMDs from groups IV–VII usually demonstrate a layered morphology that is generally presented as a crystal structure resembling graphene [44, 45]. It has been observed that the individual TMD layers have a thickness in the range of approximately 6–7 Å [44]. Since the layers in TMDs are held together by weak van der Waals forces of attraction, they serve as prime candidates for being subjected to exfoliation when appropriate techniques are applied [46].

In the MX_2 lattice, the transition metal and the chalcogen atom exhibit oxidation states of $+ 4$ and $- 2$, respectively [41]. Polymorphism exists in the few-layered form more commonly than in the bulk form. Some common polymorphs include the 1T, 2H, and 3R phases, respectively, where the letters indicate the trigonal, hexagonal, and rhombohedral orientations, respectively [41, 47]. However, for single-layered TMDs, the only two polymorphs possible are the trigonal and octahedral phases, respectively. Generally, the electronic structure of the transition metal (d-orbital) determines the polymorphic orientation, e.g., TMDs with group IV transition metals (d^0) usually crystallize in the octahedral phase, whereas those with group V transition metals (d^1) exhibit both octahedral and trigonal phases [41].

3.2 MXene

MXenes generally demonstrate the composition $M_{n+1}X_nT_x$, where M is an early transition metal (Ti, Zr, Hf, V, Nb, etc.), X is C or N and $n = 1$, 2 or 3, and T is a surface termination group (oxygen, fluorine or hydroxyl) [48]. These MXenes are generally obtained by selective leaching of the A phases out of their precursor MAX phases. The latter is a large family (approximately 70) of ternary carbides and nitrides that usually occur in layered form interspersed with group 13 and/or 14 elements separating the layers [49, 50]. Structurally, these MAX phases are alternate stacks of hexagonal MX layers with the layers of the A atoms existing in a densely packed fashion along the c-axis [51]. The type of bonding in these MAX phases is a hybrid of covalent, metallic and ionic [51].

Since the MXenes are obtained from their parent MAX phases, the M atoms are similarly arranged in a close-packed fashion with the X atoms in the octahedral interstices [52]. Generally, the MXenes exhibit a hexagonal close-packed (hcp) structure and are represented by

formulas of the type M_3C_2 (e.g., Ti_3C_2), M_4C_3 (e.g., Nb_4C_3), etc. Also, since the MXenes are synthesized by etching their precursor MAX phases, they contain the respective –OH, –O, and/or –F termination groups [48, 52]. The results of neutron scattering experiments have indicated that van der Waals bonds exist between the sheets together with hydrogen bonding between the O or OH groups within a sheet and the F group of an adjacent sheet [53]. It should also be noted the fabrication process (etching, type of etchants) strongly influences the crystallinity and the presence of defects in the final MXene product [48, 53].

3.3 Phosphorene

Phosphorene is essentially single/few layers of bulk black phosphorus and exhibits a characteristic hexagonal ("puckered honeycomb") structure [24]. The few layers are held together by weak van der Waals attractive forces. A slight variation is noticed between the lattice parameters of bulk black phosphorus ($a = 3.308$ Å, $b = 4.627$ Å, and $c = 11.099$ Å) and monolayer phosphorene ($a = 3.35$ Å and 4.62 Å) [24, 54]. The crystal structure of phosphorene is orthorhombic, and the P atom forms covalent bonds with three nearest neighbors [55]. Phosphorene demonstrates considerable anisotropy, and the stacking of its individual layers produces two orientations: the armchair and the zigzag [56].

Electronically, phosphorene behaves as a direct bandgap semiconductor. However, the application of strain may alter its semiconducting properties [57]. The number of layers making up the phosphorene sheets also influences its electronic properties [57]. Phosphorene also demonstrates anisotropic thermal properties; zigzag orientation produces size-dependent thermal behavior, while size does not play a role in the thermal behavior of the armchair oriented phosphorene [58, 59]. The surface properties of phosphorene can be tuned to exploit specific properties [60]. For example, Srivastava et al. demonstrated that a monovacancy defect causes the phosphorene atom to be magnetic whereas such an effect is not observed for divacancy defects [60, 61].

Schematic representations of the 2D materials discussed in this section together with their crystal structures, lattice parameters, and characteristic SEM and TEM images are shown in Fig. 3.

4 Fabrication of 2D Materials Relevant to Electrochemical Energy Storage Applications

The fabrication techniques of 2D materials are important since they greatly affect their final morphology, electronic properties, and even mechanical and chemical stabilities [41, 72]. There are numerous examples of reported studies on the fabrication of 2D materials in general [73]. In this section, we provide a brief summary of the fabrication techniques that are most relevant to electrochemical energy storage.

Usually, two broad empirical approaches; "top-down" and "bottom-up' are employed for the synthesis of 2D materials [13, 74]. "Top-down" techniques involve stripping away material from a bulk 3D precursor to arrive at the layered morphology, and "bottom-up" methods are useful for generating very thin (atomically) films and layers [74, 75].

One of the most straightforward top-down techniques that have been utilized for fabricating 2D materials is the mechanical exfoliation process. In this technique, individual sheets are obtained by shearing off the constituent layers of the bulk material using an applied mechanical force [76]. Phosphorene has been produced by this technique from its precursor, black phosphorus, as has many other 2D materials [24, 77, 78]. However, this technique is unreliable from a scalability perspective even though the quality of the sheets produced is generally of high purity [24, 79–81]. Another exfoliation technique that is more commonly employed is liquid phase exfoliation. In this method, the same shearing of the constituent sheets of the bulk materials takes place in a liquid media (alcohols, ketones, acids) coupled with sonication [82, 83]. The net effect is that the process helps to overcome the relatively weak van der Waals bonding that exists between the layers of the bulk parent material [73, 84]. Intercalation-assisted liquid phase exfoliation is a modified form of the liquid exfoliation technique in which a pre-lithiated bulk 2D crystal is used as the precursor. This technique has been successful in producing relatively defect free sheets [85, 86].

Another important top-down technique that is employed, especially for the fabrication of MXenes, is the etching process [22, 48]. The etching process is used to preferentially leach out the "A" atom from the precursor MAX phase of the corresponding MXene with HF used as the most common etchant [48, 87]. It should be noted that etching is strongly dependent on reaction kinetics and different MXenes have their own specific etching times [87]. Also, if etching is done in the presence of a metal halide instead of pure HF, the halide atoms tend to
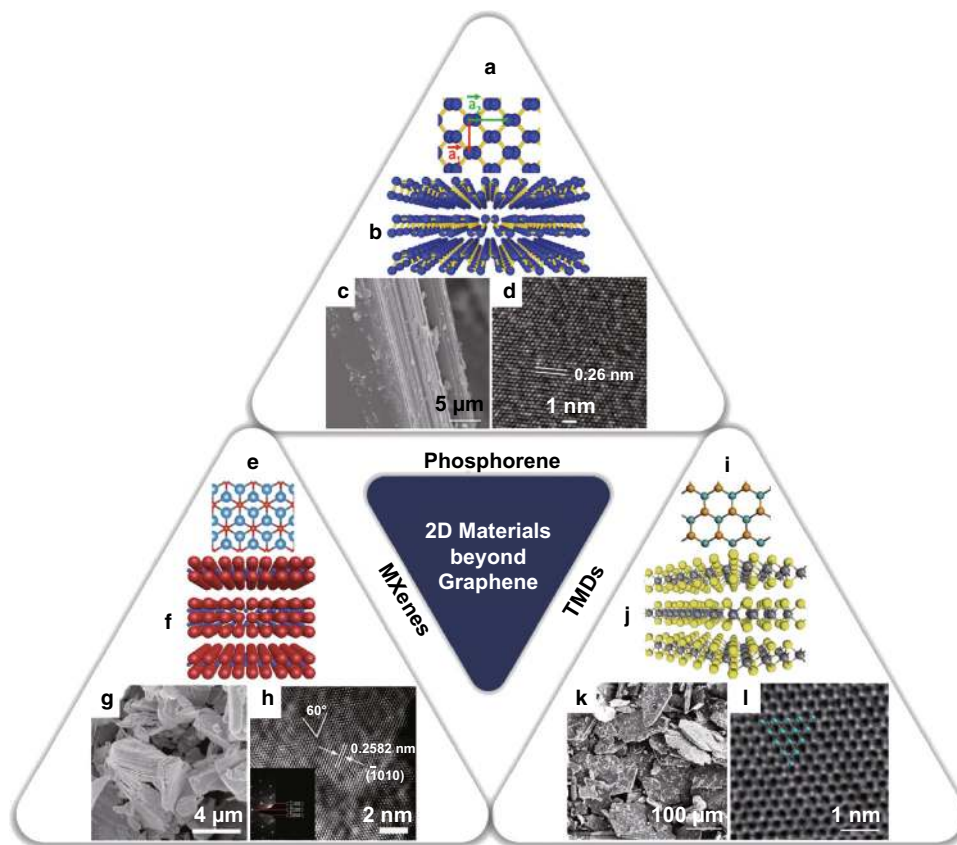
Fig. 3 Schematic representation of structure and atomic arrangement of the layered "beyond graphene" materials which are the focus of the present work: **a**, **e**, **i** Top view of the ball and stick atomic models of phosphorene, MXene, and TMD (MoSe$_2$), respectively. **b**, **f**, **j** Side view of the atomic models showing the layered structure of phosphorene, MXene, and TMD (MoSe$_2$), respectively. SEM images showing the characteristic layered structure of **c**, **g**, **k** SEM images showing the characteristic layered structure of phosphorene, MXene, and TMD (MoSe$_2$), respectively. **d**, **h**, **i** HRTEM image demonstrating the arrangement of the atoms in the lattice for phosphorene, MXene, and TMD (MoSe$_2$), respectively [24, 62–71]. Permission allowed by copyright owners

intercalate in between the MXene sheets making their exfoliation even easier [88].

Top-down techniques have been favored because of their ease of processing, low cost of materials and technique, large surface area sheets and reasonable scalability. As such, they have been widely employed for electrochemical energy storage purposes [89].

Figure 4 provides a schematic representation of the various top-down fabrication techniques.

Bottom-up techniques, e.g., chemical vapor deposition (CVD), tend to aggregate material at the most fundamental level (atoms) in a layer-wise process to produce the desired stoichiometry and morphology [90, 91]. Several bottom-up techniques have been employed in the fabrication of nanosheets; CVD and atomic layer deposition (ALD) are among the more important techniques [92, 93]. In particular, the CVD technique allows for greater control of the thickness of the final product; fabrication of the Mo$_2$C MXene crystals is a good example of this capability [94, 95]. However, bottom-up techniques are not

commonly used for electrochemical energy storage applications since they are costly, energy intensive and are not easily scalable processes. For the interested reader, detailed reviews of bottom-up approaches for 2D materials can be found in the literature by Ye et al. and Cai et al. [96, 97].

5 Performance Review of 2D Materials as Anodes in Non-Li Metal Ion Rechargeable Electrochemical Energy Storage Devices

A discussion of the fundamental electrochemistry and the performance of the various 2D materials are discussed in the subsequent sections.

5.1 Electrochemistry of 2D TMDs

In the case of 2D materials, the weak bonds between their constituent sheets and the ease of intercalation of alkali ions between their layers are two of the foremost properties
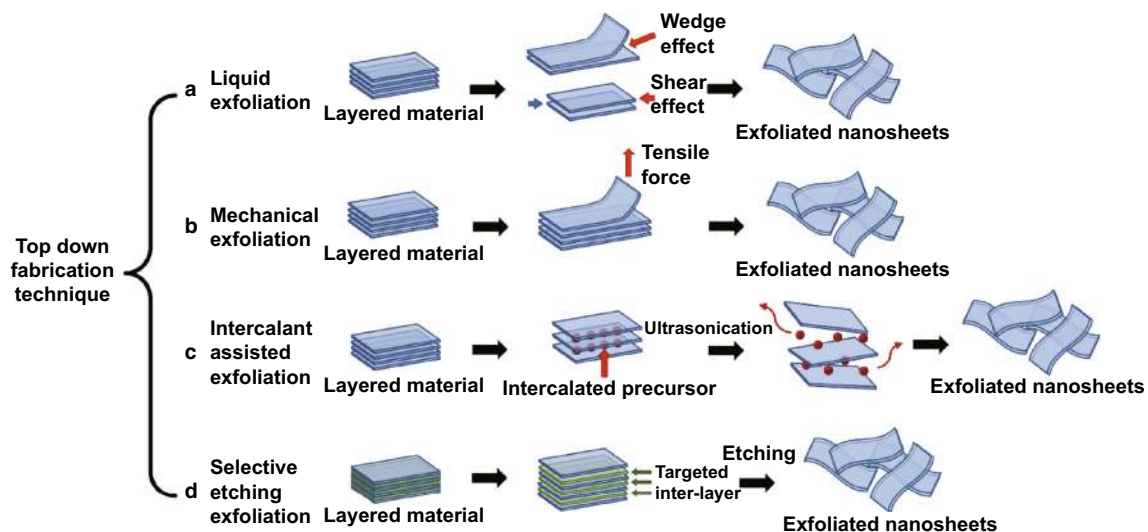
Fig. 4 Schematic representation of various "top-down" fabrication techniques for large-scale synthesis of electrode materials: **a** Liquid exfoliation where the sheets are sheared off by sonicating the bulk material in a liquid medium. **b** Mechanical exfoliation, whereby a tensile force (possibly produced by Scotch tape) can peel off the constituent layers. **c** Intercalant-assisted exfoliation where a metal ion (usually Li$^+$) is used to intercalate into the bulk precursor in a liquid media coupled with ultrasonication, which shears the sheets apart. **d** Selective etching, in which an etchant (usually strong acids, e.g., HF) is used to remove one or more constituent atoms and result in the formation of sheets

which make them desirable as energy storage materials [98]. The bulk counterparts of these layered materials suffer from significant volume changes upon interacting with alkali metal ions in addition to low average working voltages. However, when these materials are exfoliated, they are able to accommodate a greater number of inter-calating ions due to their weak out-of-plane binding [99]. Also, exfoliation increases the active surface area for electrochemical activity, reduces the tortuosity, and provides easier intercalation pathways. Among the various layered TMDs that are available, MoS$_2$ are among the most studied [100]. Manipulation of the surface properties has been shown to enhance the electrochemical behavior, as has been demonstrated by Yang et al. [101]. The vertically aligned MoS$_2$ nanosheets they synthesized exhibited a higher capacity, which is attributable to their dangling bonds which provided a greater active surface area for the ions traveling through the electrolyte [101]. Chowalla and coworkers have also demonstrated the ability of MoS$_2$ as a promising supercapacitor electrode (specific capacitance values ranging from 400 to 700 F cm^{-3}) [102]. The authors have attributed the superior performance to hydrophilicity, good electrical conductivity, and ability of the 1T MoS$_2$ to expand to host the intercalating ions [102]. Also, it has been demonstrated that some of the 2D TMDs, e.g., MoS$_2$ and WS$_2$, undergo conversion reactions, especially when interacting with Na$^+$ ions [103].

5.1.1 2D TMD Anodes for Non-Li Metal Ion Rechargeable Batteries

2D TMDs have been used as anode materials in rechargeable non-Li metal ion batteries, and the highlights of some notable performance characteristics are detailed in this section.

Ab initio studies of TMDs, primarily considering of MoS$_2$ as the template anode, have been performed to elucidate the mechanism of alkali ion interaction with the layered structure.

Mortazavi et al. used first-principles method to analyze the intercalation of Na$^+$ ions into the MoS$_2$ crystal lattice [104]. They demonstrated a phase change from 2H to 1T MoS$_2$ with the formation of intermediate Na$_x$MoS$_2$. The 2H phase was stable at all concentrations, whereas the 1T phase was only possible for $x > 0.25$ [104]. The authors have also shown the working potential to be 1.25 V. An open circuit voltage of 2.5–3.5 V is possible if coupled with a suitable positive electrode [104, 105]. Along similar lines, Li et al. performed DFT analysis together with experimental work to investigate the intermediate products formed during the process of Na$^+$ ion intercalation into MoS$_2$ [106]. They have reported on the presence of several metastable phases during the process, e.g., Na$_{0.375}$MoS$_2$, Na$_{0.625}$MoS$_2$, Na$_{1.75}$MoS$_2$. The phase transitions from 2H when Na content exceeds 0.375, with addition Na intercalation resulting in the rearrangement of the structure to the 1T morphology [106].

The application of *bare TMD nanosheets* as anode materials has been investigated by several groups. Su et al.

experimented with few-layered MoS_2 nanosheets and utilized an exfoliation technique to produce an anode for SIBs. They were able to observe a reversible specific capacity of 386 mAh g^{-1} after 100 cycles of galvanostatic charge-discharge (GCD) at an operating current density of 40 mA g^{-1} [107]. MoS_2 sheets, exfoliated in organic solvents (1-methyl-2-pyrrolidone), were studied as anodes in SIBs by Bang and coworkers [108]. First-cycle sodiation and desodiation capacities of 254 and 164 mAh g^{-1} were obtained respectively, with a Coulombic efficiency of 97% after 50 cycles [108]. An experimental analysis to study the SEI formation in a SIB with a MoS_2 nanoflake anode was performed by Lacey et al. [109]. The results indicate that an irreversible change in surface morphology occurs ("permanent wrinkling") at $\sim$ 0.4 V at the edges and the height of these undulations ranged from 7 to 36 nm [109]. The authors have attributed the undulations or "wrinkling" to the effect of Na^+ ion intercalation, with further undulations arising due to SEI formation at approximately 1.5 V [109].

WSe$_2$, in SIBs, was investigated by Share et al. They were able to obtain a reversible capacity of 200 mAh g^{-1} at a current density of 20 mA g^{-1} [110]. Ex situ results indicate the formation of isolated W and Na_xSe as intermediates during the Na ion intercalation process [110].

TMD composites have also been used to harness the overall beneficial properties of both materials. A MoS_2-rGO layered nanocomposite fabricated by a novel, facile acid-based exfoliation technique was investigated as an anode in SIB by David et al. [83]. They were able to achieve a sodiation capacity of 230 mAh g^{-1} at a current density of 25 mA g^{-1} after 20 cycles of operation [83]. A summary of the results obtained by David et al. as representative of the performance of TMD anodes, in general, is presented in Fig. 5.

A MoS_2/C composite was fabricated by Li et al. utilizing a polymethacrylate-based resin precursor, for application as an anode in SIBs [111]. A first-cycle discharge capacity of 784.3 mAh g^{-1} was achieved at current densities of 50 mA g^{-1} [111]. MoS_2 nanosheets with a preferred orientation (002 plane) grown on CNTs were studied by Zhang et al. [112]. The authors were able to achieve a specific capacity of 495.9 mAh g^{-1} at a current density of 200 mA g^{-1} with a capacity retention of 84.8% [112]. Probing of the reaction mechanism indicated that the sodiation/desodiation process was driven by a conversion reaction [112]. A novel SIB consisting of exfoliated MoS_2 nanosheets reinforced with single-walled carbon nanotubes (SWNTs) resulted in a specific capacity of approximately 420 mAh g^{-1} and only 5% capacity loss after 100 cycles of operation [113]. The authors have attributed the superior performance to the formation of a composite which greatly

improved the conductivity and formed a strong network that was deemed to be resistant to mechanical failure [113].

A layered $MoSe_2$ nanosheet structure supported by multi-walled carbon nanotubes (MWNTs) was studied by Zhang et al. as an anode in SIB [114]. A reversible specific capacity of 459 mAh g^{-1} was obtained at a current density of 200 mA g^{-1} after 90 cycles of operation [114]. The authors have proposed that a "synergistic" influence of the composites helped to produce a net improved performance compared to the individual components [114]. A $MoSe_2$ nanosheet/C cloth composite has been investigated as a flexible anode in SIBs and yielded an initial capacity as high as 452.6 mAh g^{-1} [115]. Some loss occurs in the initial cycles due to SEI formation, and 85.5% of the initial capacity is retained after 100 cycles at a current density of 0.2 A g^{-1}. The composite performs better than the bare $MoSe_2$, whose poor performance has been attributed to a lack of enhanced conducting pathways and a smaller active surface area [115]. Niu et al. studied $MoSe_2$ grown on N- and P-doped C nanosheets via a solvothermal reaction [116]. A specific capacity of 378 mAh g^{-1} was achieved after 1000 cycles of operation at a current density of 0.5 A g^{-1}, and this corresponded to a capacity retention of 87% [116]. The authors indicated that doping of the elements into the composite assisted in improving the charge transfer kinetics of the overall system [116].

TMDs have been studied as anodes in other metal ion rechargeable systems as well, albeit sparingly. A vertical MoS_2 "nanorose" grown on graphene has been investigated as an anode for application in KIB [117]. The authors reported relatively high specific capacities of 679 mAh g^{-1} at a current density of 20 mA g^{-1}. The high specific capacities were attributed to the increase in the interlayer spacing of the MoS_2 as a result of its rose pattern and composite formation with graphene [117]. WSe$_2$ for Mg ion systems has been studied by Liu and coworkers [118]. They reported a reversible specific capacity of 120 mAh g^{-1} at a high current density of 1500 mA g^{-1} with a retention of approximately 83.5% after 50 cycles [118].

A summary of the works highlighted in this section and other notable works on the application of layered 2D TMD anodes in emerging metal ion rechargeable battery systems are presented in Table 2.

5.1.2 2D TMD Electrodes for Non-Li Supercapacitors

TMDs have been applied in (aqueous) supercapacitors as well. A few prominent results will be examined in this section.

Layered MoS_2 obtained by a microwave-based heating technique loaded on rGO for support has been investigated by Firmiano and coworkers in supercapacitors [125]. A
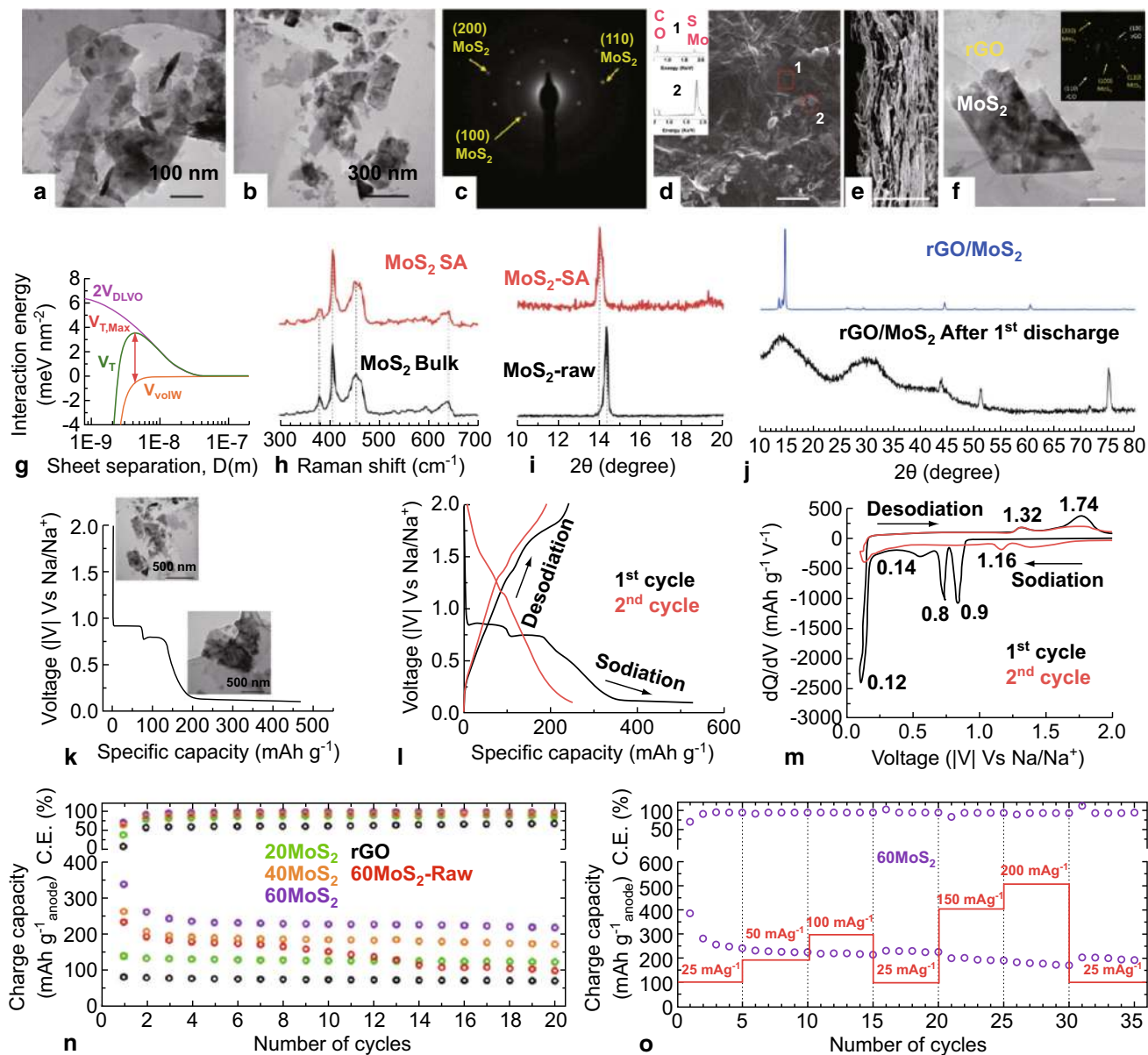
Fig. 5 Structural characterization and electrochemical performance analysis of TMD (MoS_2) as an electrode material in SIB: **a, b** HRTEM images of exfoliated MoS_2 nanosheets obtained after treatment with a superacid. **c** Selected area diffraction pattern for the MoS_2 nanosheet imaged in Fig. **b**. **d, e** SEM images of the top and cross-sectional view of the 60 MoS_2 sample (60 wt% MoS_2-40 wt% rGO), respectively. **e** TEM image of SAED pattern (in the inset) of the same 60 MoS_2 sample. **g** Graphical representation of the total interaction potential (VT), repulsion (V_{DLVO}), and attraction energy (V_{vdW}) versus greater sheet separation. **h** Raman spectra of the MoS_2 samples, in bulk (black) and after exfoliation (red) by acid treatment. **i** XRD spectra of the bulk (black) and exfoliated MoS_2 (red) sample, indicating the peak shift and the broadening of the consequent increase in the interlayer distance of the exfoliated sample. **j** XRD pattern of pristine MoS_2-rGO (60 MoS_2) electrode (blue) and the same after one discharge cycle (black). Considerable peak broadening is observed due to sodiation. **k** First discharge graph of the 60 MoS_2 electrode, also showing the formation of nanocrsytallites along the process from the TEM images and SAED patterns in the inset. **l** 1st (black)- and 2nd-cycle (red) GCD curves for the 60 MoS2 sample. **m** Differential capacity curves for the first two cycles demonstrating the redox voltages. **n** Charging capacity and Coulombic efficiency values for the different composite and bare rGO sample performed at a current density of 25 mA g^{-1}. **o** Charge capacity, coulombic efficiency, and rate capability of 60 MoS_2 sample [83]. Copyright 2014 American Chemical Society. Scale bar for **d, e** is 10 μm and for **f** is 100 nm. (Color figure online)

maximum specific capacitance of 265 F g^{-1} was obtained at a scan rate of 10 mV s^{-1} with an energy density of 63 Wh kg^{-1} [125]. A layered Mos₂-graphene composite as a supercapacitor electrode was studied by Huang et al.

[126]. A maximum specific capacitance of 243 F g^{-1} was reported by the authors in addition to an energy density of 73.5 Wh kg^{-1} [126]. The authors have attributed the observed cycling stability to efficient charge transport

Table 2 Performance of layered TMD anode, in various non-Li metal ion rechargeable battery systems

Type of TMD anode	Electrolyte chemistry	Voltage range (V)	Performance*	References
MoS_2 nanosheets	1 M $NaClO_4$ in EC/PC (1:1)	0.01–3.00	386/100/40	[107]
MoS_2 nanosheets	1 M $NaClO_4$ in FEC/PC (1:1)	0.4–2.60	161/50/0.02C[a]	[108]
WSe_2	1 M $NaPF_6$ in PC/EC/DEC (1:1:0.05)	0.10–2.50	117/30/0.1C[a]	[110]
MoS_2/graphene sheets	1 M $NaClO_4$ in DMC/EC (1:1)	0.1–2.25	218/20/25	[83]
MoS_2/C nanosheets	1 M $NaClO_4$ in EC/PC/FEC (1:1:0.05)	0.1–3.0	418.8/50/50	[111]
MoS_2/SWNT	1 M $NaClO_4$ in EC/DEC (1:1)	0.1–3.0	390/100/100	[113]
$MoSe_2$/MWNT	1 M $NaClO_4$ in EC/DMC/FEC (1:1:0.05)	0.1–3.0	459/90/200	[114]
$MoSe_2$/C cloth composite	1 M $NaClO_4$ in EC/DMC/FEC (1:1:0.05)	0.0–3.0	386.9/100/200	[115]
MoS_2/graphene "nanorose"	0.8 KPF_6 in PC/EC/FEC (1:1:0.02)	0.01–3.00	381/100/100	[117]
MoS_2/C nanosheets	1 M $NaClO_4$ in EC/DEC/PC (1:1:1)	0.01–2.90	280/300/1C[a]	[119]
MoS_2/PEO nanocomposites	$[Mg_2Cl_3]^+[AlCl_2Ph_2]^-$	0.2–2.00	75.2/30/5	[120]
$MoSe_2$ nanoplates	1 M $NaClO_4$ in PC	0.1–3.00	369/50/0.1C	[121]
WSe_2/C	1 M $NaPF_6$ in EC/DMC/FEC (1:1:0.05)	0.01–3.00	270/50/0.2C[a]	[122]
Layered MoS_2	0.5 M KPF_6 in PC/EC (1:1)	0.50–2.00	65/200/50	[123]
Layered MoS_2/rGO	$AlCl_3$-$PhMgCl$	0.01–2.10	80/50/20	[124]

*Specific capacity (mAh g^{-1})/number of cycles/current density (mA g^{-1})

[a] C rate

through the composite as well as its ability to prevent large volume expansion [126]. MoS_2/polyaniline (PANI) nanosheet composites prepared by an aniline-based intercalation process were investigated as a supercapacitor electrode by Wang et al. [127]. The composite electrode provided a specific capacitance of 390 F g^{-1} and a capacity retention of 88.6% over 1000 cycles. These composites perform significantly better than the bare PANI sample (131 F g^{-1} specific capacitance and 42% retention over 600 cycles) [127]. The authors attributed the superior result of the composite to the nanocomposite architecture which enhanced net cycling stability and conductivity [127].

Micro-supercapacitors are a relatively novel field of study. In this regard, Cao et al. designed a micron-scale supercapacitor with a thin film of layered MoS_2 as an active electrode material [128]. MoS_2 nanosheets were spray-painted on a SiO_2 substrate, and then laser patterning was performed to obtain the thin films. A volumetric capacitance of 178 F cm^{-3} and aerial capacitance of 8 mF cm^{-2} were obtained, which present reasonable performance [128]. Few-layered $MoSe_2$, prepared by a hydrothermal technique, was studied as a supercapacitor electrode by Balasingam et al. [129]. A maximum specific capacitance of 198.9 F g^{-1} was obtained with a capacitance retention of 75% after 10,000 cycles of operation [129]. Figure 6 represents a summary of the results of this group as representative of the performance of TMDs as a supercapacitor electrode.

Huang et al. studied $MoSe_2$ nanosheets on Ni foam for supercapacitor applications [130]. A very high capacity of 1114. 3 F g^{-1} with almost 100% capacitance retention after 1500 cycles was obtained [130]. A $MoSe_2$/graphene composite on Ni foam as a supercapacitor electrode was analyzed by Huang et al. The composite exhibited a specific capacity as high as 1422 F g^{-1} at a current density of 5 A g^{-1}, and 100% of the specific capacitance was retained after 1500 cycles [131]. These excellent properties were attributed to the large surface area of the composite and improvement in its electrical conductivity as well as kinetics [131].

WS_2, exfoliated by tert-butyllithium (t-Bu-Li), has shown promise as a supercapacitor material [132]. A gravimetric capacitance of 34 F g^{-1} was obtained when compared with MoS_2, $MoSe_2$, and WSe_2, which were exfoliated using the same technique [132]. This result also shows the importance of the exfoliating medium. Specifically, when WS_2 was exfoliated in a methyllithium (Me-Li) media, it exhibited a capacitance of only approximately 4 F g^{-1} [132]. Layered WS_2-rGO composite as a supercapacitor electrode material in aqueous 1 M Na_2SO_4 solution has been studied by Ratha and Rout [133]. A specific capacitance of 350 F g^{-1} was achieved at a scan rate of 2 mV s^{-1}, and the composite performed better than individual WS_2 and rGO nanosheets [133]. Table 3 gives a summary of the performance of the aforementioned layered TMDs used in supercapacitors.
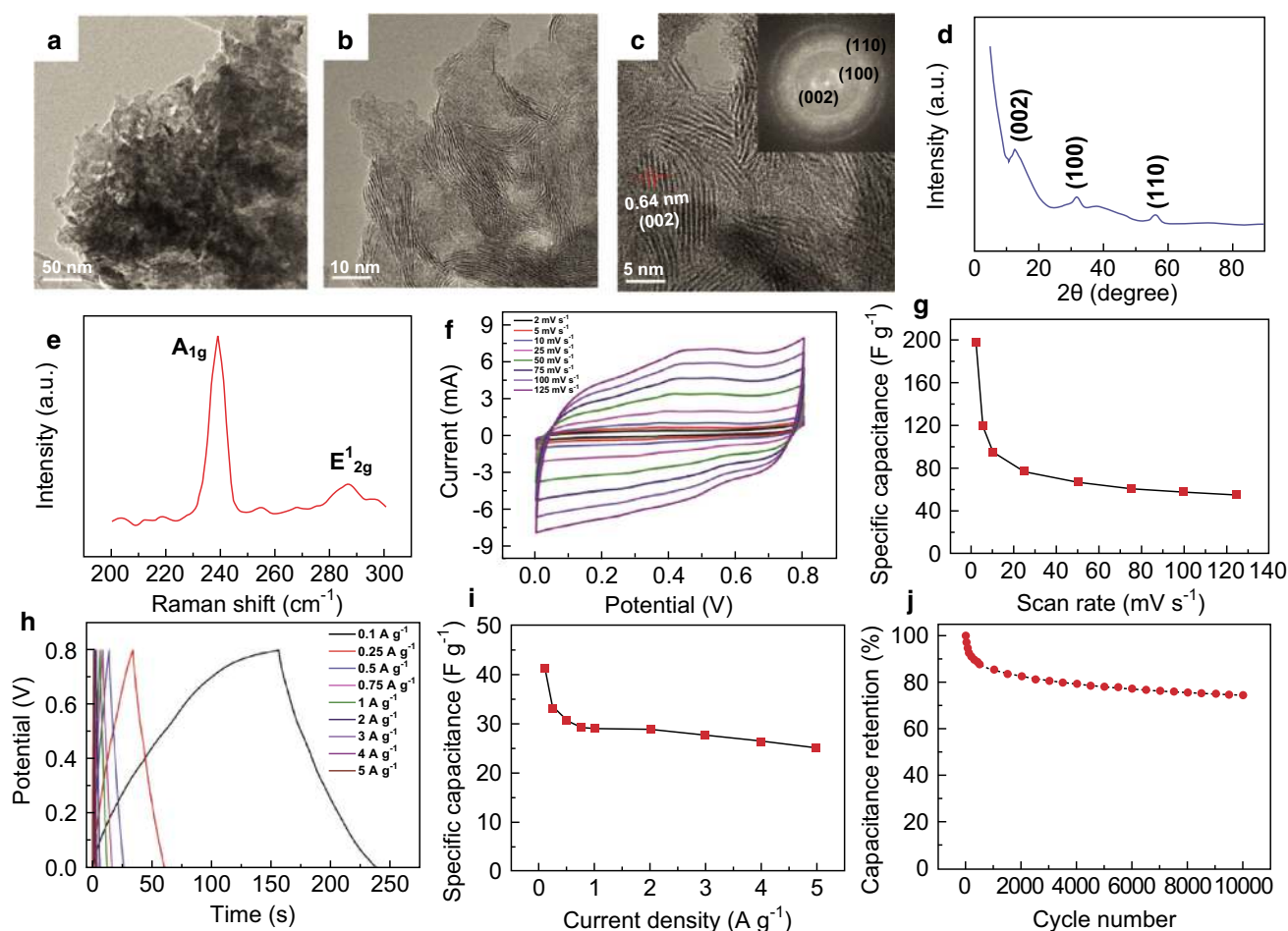
Fig. 6 Structural characterization and electrochemical performance analysis of TMD (MoSe$_2$) as a supercapacitor electrode: **a, b** TEM images of MoSe$_2$ nanosheets at low magnification. **c** HRTEM image of the MoSe$_2$ sheets with the FFT pattern demonstrated in the inset. **d** XRD spectra of the few-layered MoSe$_2$ nanosheets showing the characteristic peaks. **e** Characteristic Raman spectra of the few-layered MoSe$_2$ nanosheets where the A$_{1g}$ and E$^1_{2g}$ vibration modes are clearly visible. **f** CV of the few-layered MoSe$_2$ sample in 0.5 M H$_2$SO$_4$ with scan rates varying from 2 to 125 mV s^{-1}. **g** Corresponding specific capacitance values at the given scan rates. **h** First-cycle GCD curves at different current rates, of the few-layered MoSe$_2$ sample. **i** Specific capacitance values for the corresponding current rates. **j** Specific capacitance retention of the few-layered MoSe$_2$ sample, being run for 10,000 cycles at a current rate of 5 A g^{-1} in 0.5 M H$_2$SO$_4$ electrolyte [129]. Copyright 2015 Royal Society of Chemistry

Table 3 Performance of layered 2D TMD electrodes in various non-Li supercapacitor systems

Type of TMD	Electrolyte chemistry	Performance*	References
MoS$_2$/rGO	1 M HClO$_4$	265 F g^{-1}/10 mV s^{-1}	[125]
MoS$_2$/graphene	1 M Na$_2$SO$_4$	243 F g^{-1}/1 A g^{-1}	[126]
MoS$_2$	1 M NaOH	178 F cm^{-3}/10 mV s^{-1}	[127]
MoS$_2$/PANI	1 M H$_2$SO$_4$	390 F g^{-1}/0.8 A g^{-1}	[128]
MoSe$_2$	0.5 M H$_2$SO$_4$	199 F g^{-1}/2 mV s^{-1}	[129]
MoSe$_2$	6 M KOH	1114.3 F g^{-1}/1 A g^{-1}	[130]
MoSe$_2$/graphene	6 M KOH	1422 F g^{-1}/5 A g^{-1}	[131]
WS$_2$	0.1 M 7.4 pH PBS	40 F g^{-1}/0.5 A g^{-1}	[132]

*Specific capacitance (F g^{-1})/scan rate (mV s^{-1})

5.2 Electrochemistry of MXenes

MXenes presents a low diffusion barrier for intercalation of various alkali metal ions between their sheets and therefore is not suitable for application as negative electrode materials in non-Li ion rechargeable battery systems [48]. However, depending on the fabrication technique and the type of terminating agent, various MXenes can function in a range of potential windows, thereby providing considerable flexibility in terms of their performance [48]. It has been observed that MXenes of the general formula M_2X tend to demonstrate greater specific capacities than the ones with their corresponding higher molecular weight counterparts such as M_3X_2 and M_4X_3, since the low-formula-weight MXenes can store a greater number of ions [134]. The presence of the terminating functional group has been demonstrated to significantly affect the net specific capacity exhibited by the MXene, e.g., MXenes with oxygen-containing terminating groups exhibit much larger specific capacity than those with fluorine-containing groups [135]. The addition of intercalating particles between the MXene sheets has been shown to greatly enhance their specific capacity and electrode longevity [136].

5.2.1 MXene Anodes for Non-Li Metal Ion Rechargeable Batteries

A first-principles study of M_2C-type MXene (where M = transition metal such as Ti, V, Cr etc.) as a Na-ion battery anode was performed by Yang et al. using density functional theory (DFT) [65]. The results revealed a low anode voltage (< 1.5 V) and activation energy (0.09–0.18 eV) for Na ion migration in MXenes which suggests a high energy density and high rate capability [65]. Along similar lines, the intercalation of different alkali ions (Na, K and Ca) into Ti_3C_2 were studied by Er et al. Theoretical specific capacities of 351.8, 319.8, and 191.8 mAh g^{-1} were obtained for Na, Ca and K, respectively, and reported by the authors [137]. Theoretical DFT-based studies on the applicability of Mo_2C monolayers have been recently performed by Sun and coworkers [138]. They have demonstrated diffusion barriers of 0.0035 and 0.0015 eV for Li and Na atoms, respectively, into the Mo_2C monolayer lattice, indicating the probability of good diffusion and superior charge and discharge rates [138].

Experimental results for the electrochemical performance of MXene (Ti_3CNT_x) as an anode material was reported by Naguib et al. for the K-ion battery [139]. For the first cycle, 202 mAh g^{-1} capacity recovered was achieved (with 28.4% coulombic efficiency, 1.5 K$^+$ correlation) which continuously degraded to 75 mAh g^{-1} after 100 cycles (with 0.6 K$^+$ correlation) [139]. Natu et al. studied the influence of pH variation during fabrication of

2D MXenes [140]. Crumpled mesoporous MXene (Ti_3C_2-T_x) flakes were synthesized via a reduction in the pH of the MXene suspension. A sodium ion battery using this electrode as an anode resulted in specific capacities of 250 and 120 mAh g^{-1} at 20 and 500 mA g^{-1}, respectively [140]. In order to avoid restacking behavior and to improve the limited capacity of bare MXene, Wu et al. recently proposed an efficient technique which involved the insertion of SnS_2 nanoplates between MXenes ($Ti_3C_2T_x$) interlayers [141]. The MXene/SnS_2 composites were synthesized by self-assembly of sonicated MXene suspension and hydrothermal-synthesized SnS_2. Electrochemical measurements revealed a capacity retention of 120 mAh g^{-1} for a 100 mA g^{-1} current density after 125 cycles at 0 °C for a MXene/SnS_2 5:1 (mass ratio) electrode [141]. In another investigation by the same group, MoS_2 nanosheets were used as intercalation particles between MXene ($Ti_3C_2T_x$) layers [142]. The MXene/MoS_2 composite resulted in a reversible capacity of 250.9 mAh g^{-1} after 100 cycles, while 162.7 mAh g^{-1} could be retained as the capacity at 1 A g^{-1}, indicating a high rate capability [142]. Similarly, a MXene/Sb_2O_3 composite material was developed by Guo et al. through a facile solution phase fabrication technique [143]. The specific capacities of the as-prepared composite material as anodes for Na-ion batteries were measured to be as high as 472 mAh g^{-1} at 100 mA g^{-1} after 100 cycles. It also exhibited a high rate capability of 295 mAh g^{-1} at 2 A g^{-1} as well [143].

MXenes (Ti_3C_2) have also been used as precursors to fabricate Na or K containing titanate nanoribbons as anodes by Dong et al. under the alkalization effect of NaOH or KOH [144]. These ultrathin ribbons presented 191 mAh g^{-1} (Na titanate) for the Na-ion battery at 200 mA g^{-1}. Likewise, 151 mAh g^{-1} (K titanate) was achieved for the K-ion battery at 50 mA g^{-1} [144]. Lian et al. studied an alkalized Ti_3C_2 MXene nanoribbon for SIB and KIB systems [145]. The MXene produced a specific capacity of 42 mAh g^{-1} for the KIB system after 500 cycles of operation and the authors have attributed the superior results to the enhanced interlayer spacing which allows for storage of more ions [145]. A summary of Lian's results is presented in Fig. 7, which is representative of the performance of MXene anodes in KIB systems.

Table 4 provides a list of the various notable MXene anode performances in emerging metal ion rechargeable battery systems.

5.2.2 MXene Electrodes for Non-Li Supercapacitors

MXenes have also been exploited for use as electrodes in supercapacitors due to their excellent cyclability and high capacitance [67]. Xu et al. obtained binder-free MXene ($Ti_3C_2T_x$) nanoflakes using a modified electrophoretic
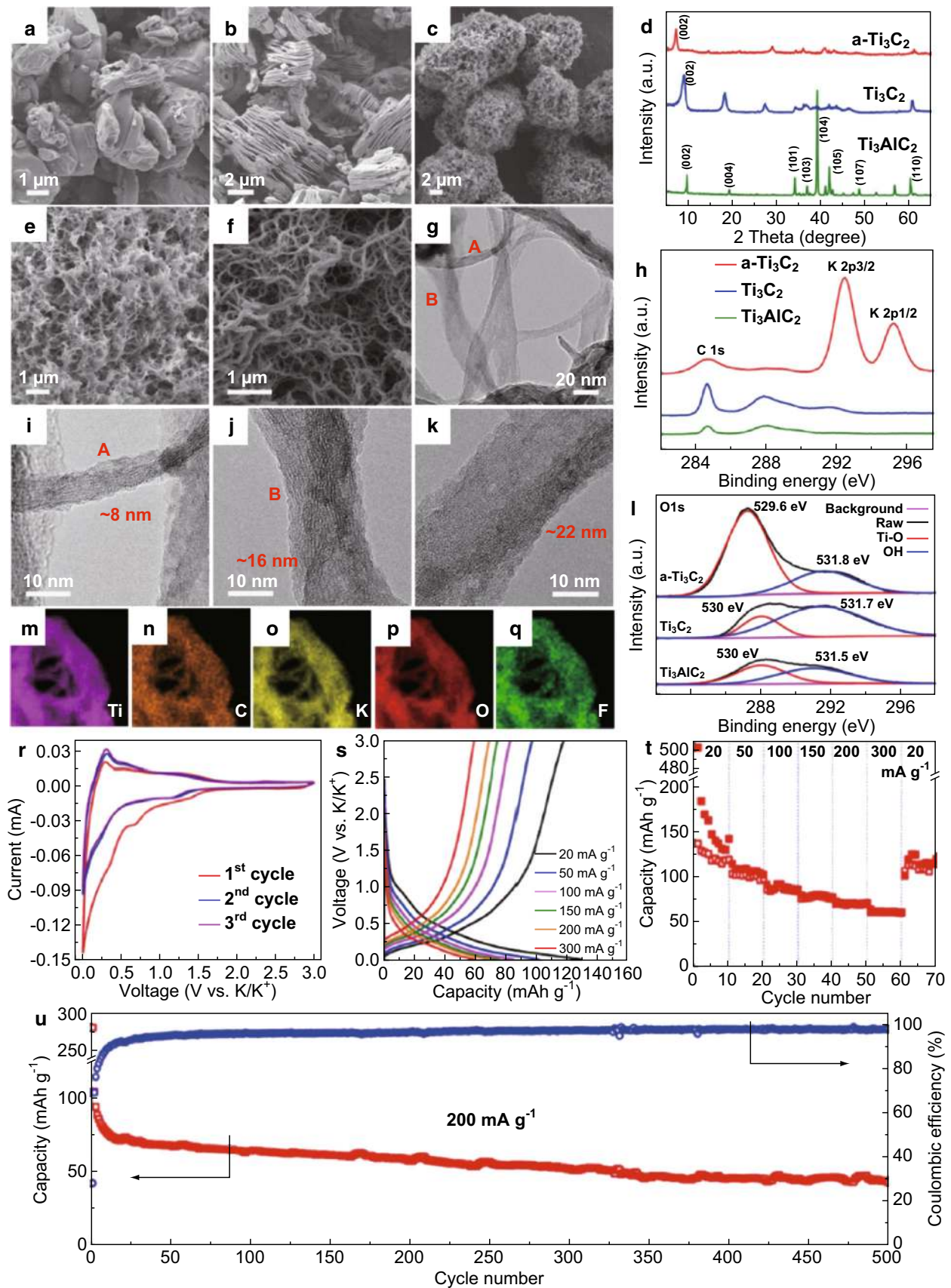
◀**Fig. 7** Structural characterization and electrochemical performance analysis of MXene as electrode material in KIB: **a–c** SEM images of Ti_3AlC_2 MAX phase, Ti_3C_2 MXene nanosheets (MNSs) obtained by etching the precursor MAX phase with 40% HF solution and KOH-treated Ti_3C_2 MNSs (a-Ti_3C_2), respectively. **d** XRD spectra stack of Ti_3AlC_2, Ti_3C_2 and a-Ti_3C_2. **e** SEM image of Ti_3C_2 MXene nanoribbons (MNRs) at low magnification. **f** Corresponding image at high-magnification **g** TEM image of MNRs h XPS spectra of Ti_3AlC_2, Ti_3C_2, and a-Ti_3C_2 showing the free C and K peaks. **i–k** HRTEM images of the Ti_3C_2 MNRs at different positions ("A" and "B") and varying thicknesses (8, 16, and 22 nm). **l** XPS spectra of the 3 samples showing the O 1s peak. **m–q** Elemental mapping of Ti, C, K, O and F regions of the a-Ti_3C_2 sample, respectively. **r** CV of the a-Ti_3C_2 MNRs for KIB collected at a scan rate of 0.1 mV s^{-1}. **s** GCD curves of the sample obtained at different given current rates. **t** Rate capability for the a-Ti_3C_2 sample. **u** Cycling performance at 200 mA g^{-1} and coulombic efficiency for the a-Ti_3C_2 sample [145]. Copyright 2018 Elsevier

deposition (MEPD) method. The MXene films were then self-assembled on nickel foam. The flexible solid-state supercapacitor using as-prepared MXene electrodes demonstrated a specific capacitance of 140 F g^{-1} in 1 M KOH without capacitance degradation after 10,000 cycles. Ti_3C_2 MXene was prepared by Gao et al. from Ti_3AlC_2 via selective etching of Al in HF, resulting in a surface area of 22.34 m^2 g^{-1} [149]. Electrochemical characterization showed a volumetric capacitance of 119.8 F cm^{-3} in 3 M KOH electrolyte at 2.5 A g^{-1} which retained 94.2% (112.9 F cm^{-3}) after 1000 cycles. This performance can be conveniently improved by elemental doping according to Wen et al., such as N-doped the procedure of $Ti_3C_2T_x$ which was proposed in their research [150]. Annealing MXene in flowing ammonia at a temperature of 200–700 °C provided concentration-controlled N-$Ti_3C_2T_x$ with nitrogen contamination of 1.7–20.7 at%. A significantly elevated specific capacitance of 192 F g^{-1} was obtained, compared to 34 F g^{-1} from a pure $Ti_3C_2T_x$ anode, in the same 1 M H_2SO_4 electrolyte [150]. The main results of this work are shown in Fig. 8 as a representative example of MXene's performance as a supercapacitor electrode. Another investigation by Wang et al. demonstrated that an even superior specific capacitance of 1061 F g^{-1} at 1 A g^{-1} achieved using (Ti_3C_2)/Ni-Al double-layer hydroxide composite with high rate capability achieved a specific capacitance of 556 F g^{-1} at 10 A g^{-1} [151].

Table 5 lists the performance of several notable MXenes which have been used for non-Li supercapacitor applications.

5.3 Electrochemistry of Phosphorene

Phosphorene, single/few layers of black phosphorus has demonstrated a high theoretical specific capacity (2596 mAh g^{-1} for Li$^+$ ions); however, large volume expansion on interaction with intercalating ions remains an important concern [157, 158]. Theoretical studies have demonstrated an anisotropic intercalation of Na$^+$ ions into phosphorene, which can be attributed to its puckered honeycomb-like structure [159]. Density functional studies have also demonstrated that adsorption of alkali ions, especially Na$^+$ ions, usually occurs on both sides of the phosphorene sheet [159]. Since adsorption over adjacent sides reduces the net repulsion, this arrangement is favored over ionic adsorption for a single side [159]. Several intermediate metastable phases have been reported, especially for Na$^+$ ion intercalation, e.g., NaP_8, NaP_2, and are observed during the cycling of phosphorene anode [26, 160].

Table 4 Performance of MXene electrodes, in various non-Li metal ion rechargeable battery systems

Type of MXene	Electrolyte chemistry	Voltage range (V)	Performance*	References
Ti_3CNT_x	0.8 M KPF_6 in EC/DEC (1:1)	0.005–3	75/100/20	[139]
$Ti_3C_2T_x$	1 M $NaClO_4$ in EC/PC/FEC (1:1:0.05)	0.001–3	246/50/20	[140]
$Ti_3C_2T_x$	1 M $NaClO_4$ in EC/PC (1:1)	0.01–2.5	322/200/100	[141]
$Ti_3C_2T_x$	1 M $NaPF_6$ in EC/DEC (1:1)	0.1–3	100/100/20	[146]
$Ti_3C_2T_x$/MoS_2	1 M $NaClO_4$ in EC/PC (1:1)	0.01–3	250.9/100/100	[142]
$Ti_3C_2T_x$/Sb_2O_3	1 M $NaClO_4$ in EC/PC (1:1)	0.01–2.5	472/100/100	[143]
Ti_3C_2 ribbon	1 M $NaCF_3SO_3$	0.01–3	113/200/50	[145]
Ti_3C_2 ribbon	0.8 M KPF_6	0.01–3	42/500/200	[145]
$Ti_3C_2T_x$/CTAB	0.4 $(PhMgCl)_2$-$AlCl_3$/THF	0.01–2	135^a/250/20	[147]
$Ti_3C_2T_x$/CNT	1 M $NaClO_4$ in EC/PC/FEC (1:1:0.05)	0.01–3	164/100/50	[148]
Sn-Ti_3C_2	1 M $LiPF_6$ in EC/PC (1:1)	0.01–3	500/200/500	[136]

*Specific capacity (mAh g^{-1})/number of cycles/current density (mA g^{-1})

^{a}Volumetric capacity (mAh cm^{-3})
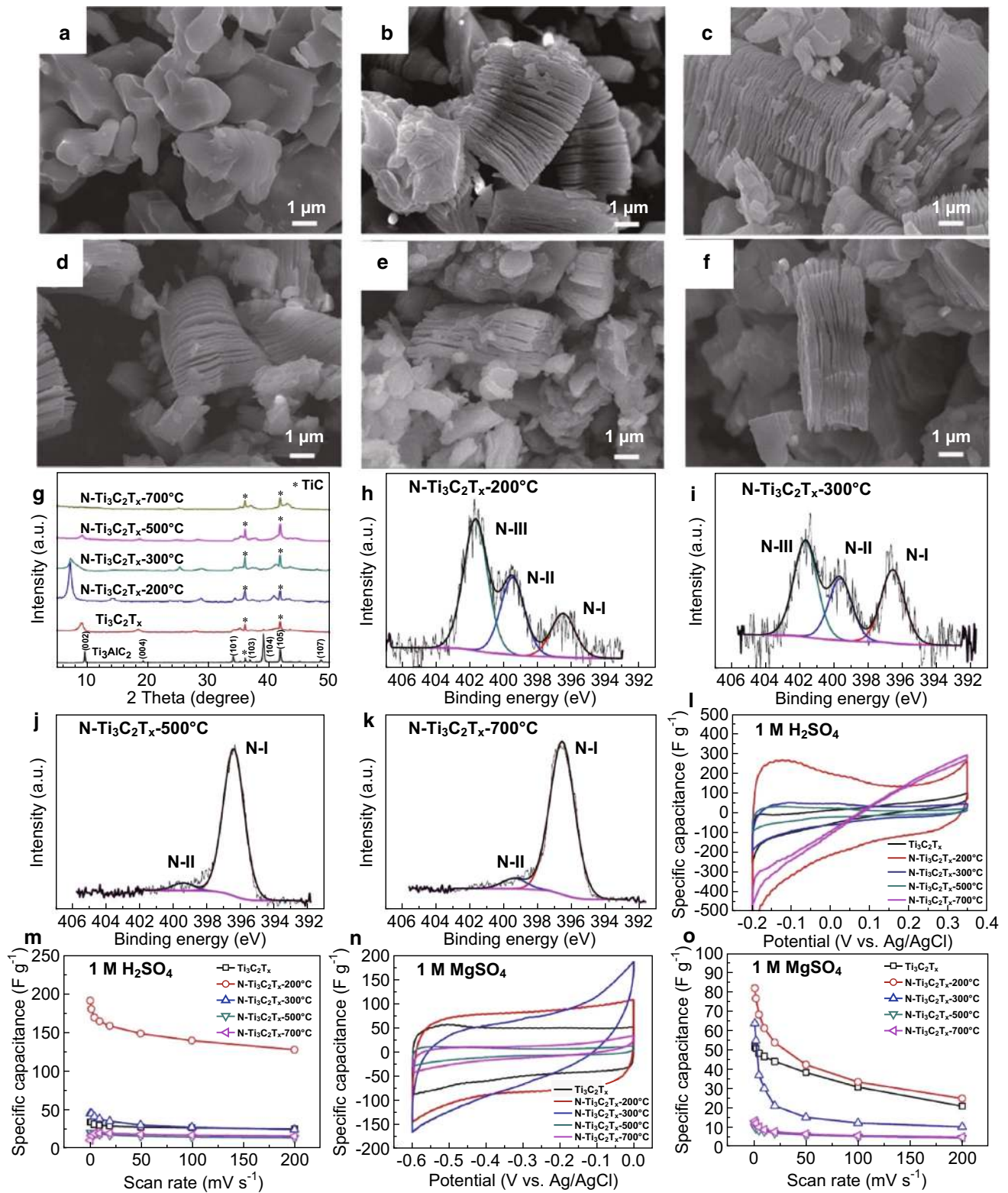
◄**Fig. 8** Structural characterization and electrochemical performance analysis of MXene (N-doped $Ti_3C_2T_x$) as a supercapacitor electrode: SEM images of **a** Parent MAX phase Ti_3AlC_2. **b** $Ti_3C_2T_x$ obtained after etching the MAX phase with HF. **c** N-doped Ti_3C_2Tx synthesized at 200 °C (N–$Ti_3C_2T_x$-200 °C). **d** N–$Ti_3C_2T_x$-300 °C. **e** N–$Ti_3C_2T_x$-500 °C. **f** N–$Ti_3C_2T_x$-700 °C. **g** XRD spectra stack of the parent MAX phase (Ti_3AlC_2) and the non-doped and various N-doped $Ti_3C_2T_x$ MXenes. **h–k** XPS spectra of N–$Ti_3C_2T_x$-200 °C, N–$Ti_3C_2T_x$-300 °C, N–$Ti_3C_2T_x$-500 °C, N–$Ti_3C_2T_x$-700 °C samples, respectively. **l** CV curves of the non-doped and doped MXenes in 1 M H_2SO_4 at 1 mV s^{-1} scan rate. **m** Specific capacitance of the MXenes corresponding to the scan rates in **i** and **n** CV curves of the non-doped and doped MXenes in 1 M $MgSO_4$ at 1 mV s^{-1} scan rate. **o** Specific capacitance of the MXenes corresponding to the scan rates in **n** [150]. Copyright 2018 Elsevier

5.3.1 Phosphorene Anodes for Non-Li metal Ion Rechargeable Batteries

Some notable studies on phosphorene anodes in non-Li metal ion rechargeable batteries are outlined in the following discussion.

Kulish et al. performed a theoretical study of phosphorene for SIB systems and reported a maximum theoretical specific capacity of 865 mAh g^{-1} with a resultant NaP stoichiometry [159]. Layered BP, essentially the precursor of phosphorene, has been studied as an anode in SIBs by Peng and coworkers [161]. The researchers essentially used a BP-carbon black nanocomposite anode were able to achieve 1381 mAh g^{-1} after 100 cycles of operation at a rate of 90.5%. Increased conductivity and the enhanced electroactive surface area of the nanocomposite played a decisive role in facilitating such high capacities, according to the authors [161]. BP-graphitic composite anodes in KIBs have been studied by Sultana et al. The first-cycle specific capacity obtained was 617 mAh g^{-1}, which is more than twice that of pristine graphite for SIBs with 61% retention over 60 cycles of operation. The authors proposed an alloying reaction mechanism for the anode. It was

determined that the composite with a weight ratio BP/C of 1:1 performed best [162].

Nie et al. reported a maximum discharge capacity of 2631 mAh g^{-1} with a Coulombic efficiency of 77% for phosphorene as a SIB anode [163]. The authors were able to probe the movement of the Na$^+$ ion into the phosphorene lattice and have provided a model for this behavior [163]. Figure 9 represents a description of the mechanism and the performance of phosphorene as an anode in SIBs.

A phosphorene-graphene (P/G) hybrid anode in SIB systems has been studied by Sun et al. [164]. The authors have identified a 2-step intercalation-alloying mechanism that helps to produce an elevated specific capacity of 2440 mAh g^{-1} at a current density of 50 mA g^{-1} with a capacity loss of only 15% after 100 cycles of operation [164]. Hexagonal boron nitride (h-BN)-capped phosphorene (h-Bn/Pn) as an anode for SIBs was investigated using ab initio techniques by Chowdhury and coworkers [165]. A reversible specific capacity of 445 mAh g^{-1} was obtained with a binding energy of 2.55 eV for Na$^+$ ions in h-BN/Pn [165].

Theoretical studies for phosphorene as anodes in Mg ion batteries have demonstrated a diffusion barrier of 0.08 eV with an alloying reaction mechanism and an $Mg_{0.5}P$ intermediate [166].

The performance of notable BP/phosphorene systems as anodes in emerging non-Li metal ion rechargeable batteries is provided in Table 6.

5.3.2 BP/Phosphorene Electrodes for Non-Li Supercapacitors

A composite of BP nanoflakes/PANI in pseudocapacitors has been investigated by Sajedi-Moghaddam et al. [170]. A high specific capacitance of 354 F g^{-1} was achieved by the nanocomposite, at a current density of 0.3 A g^{-1}. According to the authors, the large surface area generated by the layered BP allowed the PANI to nucleate which

Table 5 Performance of MXene electrodes in various non-Li supercapacitor systems

Type of MXene	Electrolyte chemistry	Performance*	References
$Ti_3C_2T_x$ film	1 M KOH	140 F g^{-1}/5 mV s^{-1}	[67]
Ti_3C_2	3 M KOH	119.8 F cm^{-3}/2.5 A g^{-1}	[149]
N–$Ti_3C_2T_x$	1 M H_2SO_4	192 F g^{-1}/1 mV s^{-1}	[150]
Ti_3C_2/Ni–Al	6 M KOH	1061 F g^{-1}/1 A g^{-1}	[151]
$Ti_3C_2T_x$/rGO	1 M $MgSO_4$	435 F cm^{-3}/2 mV s^{-1}	[152]
$Ti_3C_2T_x$/rGO	3 M H_2SO_4	1040 F cm^{-3}/2 mV s^{-1}	[153]
$Ti_3C_2T_x$ film	EMI-TFSI	70 F g^{-1}/20 mV s^{-1}	[154]
Ti_2CT_x–N_2/H_2	30 wt. % KOH	51 F g^{-1}/1 A g^{-1}	[155]
Ti_3C_2	1 M KOH	76 F g^{-1}/2 mV s^{-1}	[156]

*Specific capacitance (F g^{-1})/scan rate (mV s^{-1})
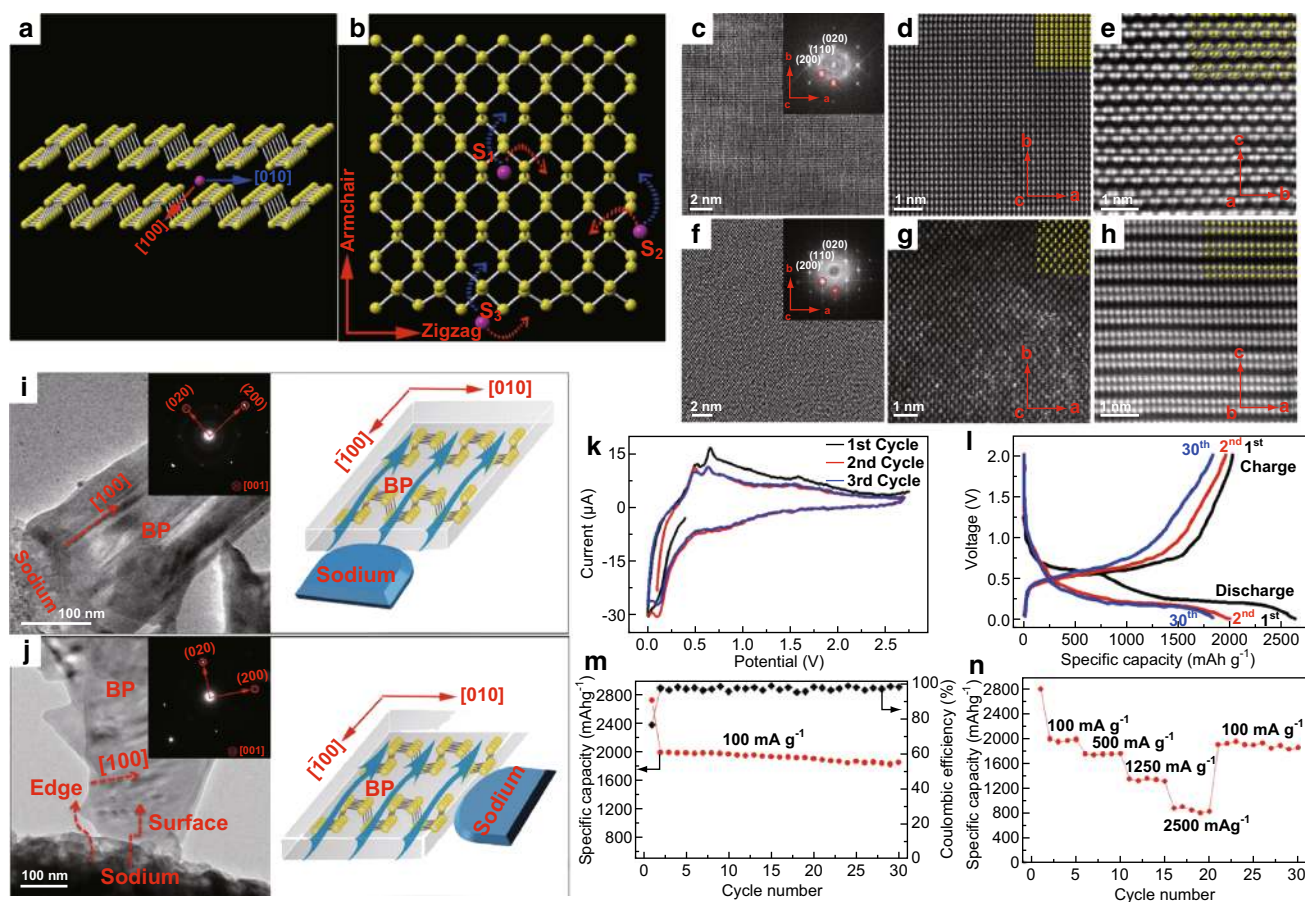
Fig. 9 Structural characterization and electrochemical performance analysis of phosphorene electrode material in SIB: **a** Schematic showing the movement of Na$^+$ ion between phosphorene layers. **b** Energetics dictated transport of Na$^+$ ions in the interstices of phosphorene lattice. **c**, **f** HRTEM images along the [001] direction of few-layer phosphorene and single-layer phosphorene, respectively, with FFTs shown in the inset of each. **d**, **g** Atomic-scale high-angle annular dark field image (HAADF) along the [001] direction of few-layer phosphorene and single-layer phosphorene, respectively, with atomic orientations in inset (in yellow). **e**, **h** HAADF of few-layer phosphorene along the [100] and [010] directions, respectively, with the corresponding atomic orientations in the inset (in yellow). **i**, **j** TEM image and schematic of the contact interface of Na$^+$ ion normal to the [100] direction and along the [100] direction, respectively. The SAED patterns of the few-layered phosphorene are shown in the inset of both. **k** CV of the first three cycles of the phosphorene electrode for the half cell at a scan rate of 0.005 mV s^{-1}. **l** GCD profiles of the 1st, 2nd, and 30th cycle for the phosphorene electrode in the half cell. **m** Capacity retention and coulombic efficiency of the phosphorene electrode running at a current density of 100 mA g^{-1}. **n** Rate capability of the phosphorene anode [163]. Copyright 2016 American Chemical Society. (Color figure online)

produced a greater number of ion channels facilitating enhanced charge storage [170].

Exfoliated BP nanoflakes have been investigated in all-solid-state supercapacitors by Hao et al. [171]. A net stack capacitance of 45.8 F g^{-1} was obtained at a scan rate of 0.01 V s^{-1} with a capacitance retention of 71.8% after 30,000 cycles of operation [171]. Along the same lines, Yang and coworkers used a composite of BP nanoflake/CNT paper as an all-solid-state supercapacitor [172]. A maximum volumetric capacitance of 41.1 F cm^{-3} was obtained at a voltage scan rate of 0.005 V s^{-1}, whereas a power density of 821.62 W cm^{-3} was obtained at a scan rate of 500 V s^{-1}, indicating its robust performance [172]. A nanocomposite with a BP/CNT weight ratio of 1:4 provided the best results [172]. Luo et al. studied a

polypyrrole/BP-laminated film composite as an electrode in a flexible solid-state supercapacitor and obtained a maximum specific capacitance of 497.5 F g^{-1} and almost 100% capacitance retention after 10,000 cycles at a current density of 5 A g^{-1} [173]. The authors attributed the superior performance to the lamination which provided an easier path for the ions and also prevented structural degradation during cycling [173].

Scientific research on phosphorene as an electrode in supercapacitors has been sparingly performed. As a notable exception, Xiao et al. studied a phosphorene-graphene (P/G) interdigital micro-supercapacitor in an ionic liquid environment [174]. A conductivity of 319 S cm^{-1} and an energy density value of 11.6 mWh cm^{-3} were reported by the authors [174]. Figure 10 represents a

Table 6 Performance of BP/phosphorene anode, in various non-Li metal ion rechargeable battery systems

Type of Phosphorene	Electrolyte chemistry	Voltage range	Performance*	References
Phosphorene	N.A.	N.A.	433 for NaP$_2$ stoichiometry[a]	[159]
P/C composite layers	1 M NaClO$_4$ in EC/PEC/FEC (1:1:0.1)	0.005–1.5 V	1500/100/100	[161]
Layered black phosphorus	0.75 M KPF$_6$ in EC/DEC (1:1)	0.01–2.00 V	400/50/50	[162]
P/G hybrid	1 M NaPF$_6$ in EC/DEC/FEC (1:1:0.1)	0.00–1.50 V	2400/100/0.02C[b]	[164]
Layered black phosphorus	1 M NaPF$_6$ in EC/DEC (1:1)	0.00–2.00 V	1500/25/125	[167]
P/G hybrid layers	N.A.	Sodiation between 0.29 and 0.70 V	372[b]	[168]
Phosphorene	N.A.	N.A.	410 for 50% Mg intercalation[a]	[169]
Phosphorene	N.A.	N.A.	310.71 for Mg$_{0.5}$P[a]	[26]

*Specific capacity (mAh g^{-1})/number of cycles/current density (mA g^{-1})

[a]Specific capacity (mAh g^{-1}) for theoretical study

[b]C rate

summary of their results, as representative of the application of phosphorene in non-Li supercapacitors. Flexible double electrodes of phosphorene for supercapacitor applications have resulted in a specific capacitance of 13.75 F cm^{-2} and an energy density of 2.47 mWh cm^{-3} for a scan rate of 0.01 V s^{-1} [175]. A tabular listing of the performance of BP/phosphorene electrodes as non-Li supercapacitors is provided in Table 7.

6 Comparison, Challenges, and the Path Forward

This review has examined the novel properties of 2D materials and illustrated some of their notable applications as rechargeable non-Li metal ion battery anodes and supercapacitor electrodes. However, there are also many challenges associated with the use of 2D materials and important research is being pursued to address them. A few of these limitations will be briefly summarized in the subsequent paragraphs in this section regarding each class of 2D material discussed in this article.

TMDs have received the most attention among the various 2D materials reviewed. MoS$_2$, the foremost among them, has an interlayer spacing (0.65 nm) large enough to facilitate facile intercalation of Na$^+$, K$^+$ ions. It also provides a high theoretical capacity (670 mAh g^{-1}) for sodium storage [176]. In practice, capacities as high as 530 mAh g^{-1} have been obtained for standalone MoS$_2$ systems [107]. However, it is observed that the intercalation of large monovalent alkali metals (e.g., Na$^+$, K$^+$) into its constituent layers cause significant structural change [177]. This, coupled with the fact that these materials tend to undergo conversion reactions (especially with Na$^+$ ionic intercalation), results in the formation of soluble polysulfides which might have undesirable side reactions with the electrolyte [177]. Several techniques have been considered to address these issues such as nanocrystallization, electrode modification, carbon modification. Among these techniques, carbon modification of the MX$_2$ TMDs has been studied most exhaustively and it includes the creation of a composite of the TMD with carbon nanotubes, carbon nanoparticles, etc. [177, 178]. This helps to improve porosity, reduce diffusion pathways, and provide a stable support [177, 178]. Controlling the working voltage to prevent the formation of undesirable side products is another technique that has been investigated [177]. In the case of selenides, another issue which has been investigated is cycling stability [179]. To overcome these shortcomings, nanocomposites with carbon-based materials or doping of the selenides have been proposed [179]. Restacking of the TMD sheets, especially for IT-MoS$_2$, is an issue that is frequently encountered [180]. Spacers in the form of graphene or carbon nanotubes are introduced between the TMD sheets, and the hybrid structure also has enhanced kinetics [181]. The deadweight of the binder and the current collector are undesirable additives that tend to reduce the gravimetric and volumetric capacitance. To overcome this problem, free-standing electrodes have been studied [83].

MXenes too suffer from similar problems of irreversible aggregation and stacking. The incorporation of graphene or conducting polymers between the interlayers has been demonstrated to prevent this problem to a large extent [13]. The use of MXenes in organic electrolytes also poses some challenges, which can also be rectified using conducting spacers, e.g., carbon nanotubes to improve the kinetics and rate performance [48]. Recently, MXene electrodes have also demonstrated notable performance in ionic liquid electrolytes [48, 154]. Another important challenge is to produce MXenes with no surface functional groups. CVD techniques have been proposed to achieve this objective [48].
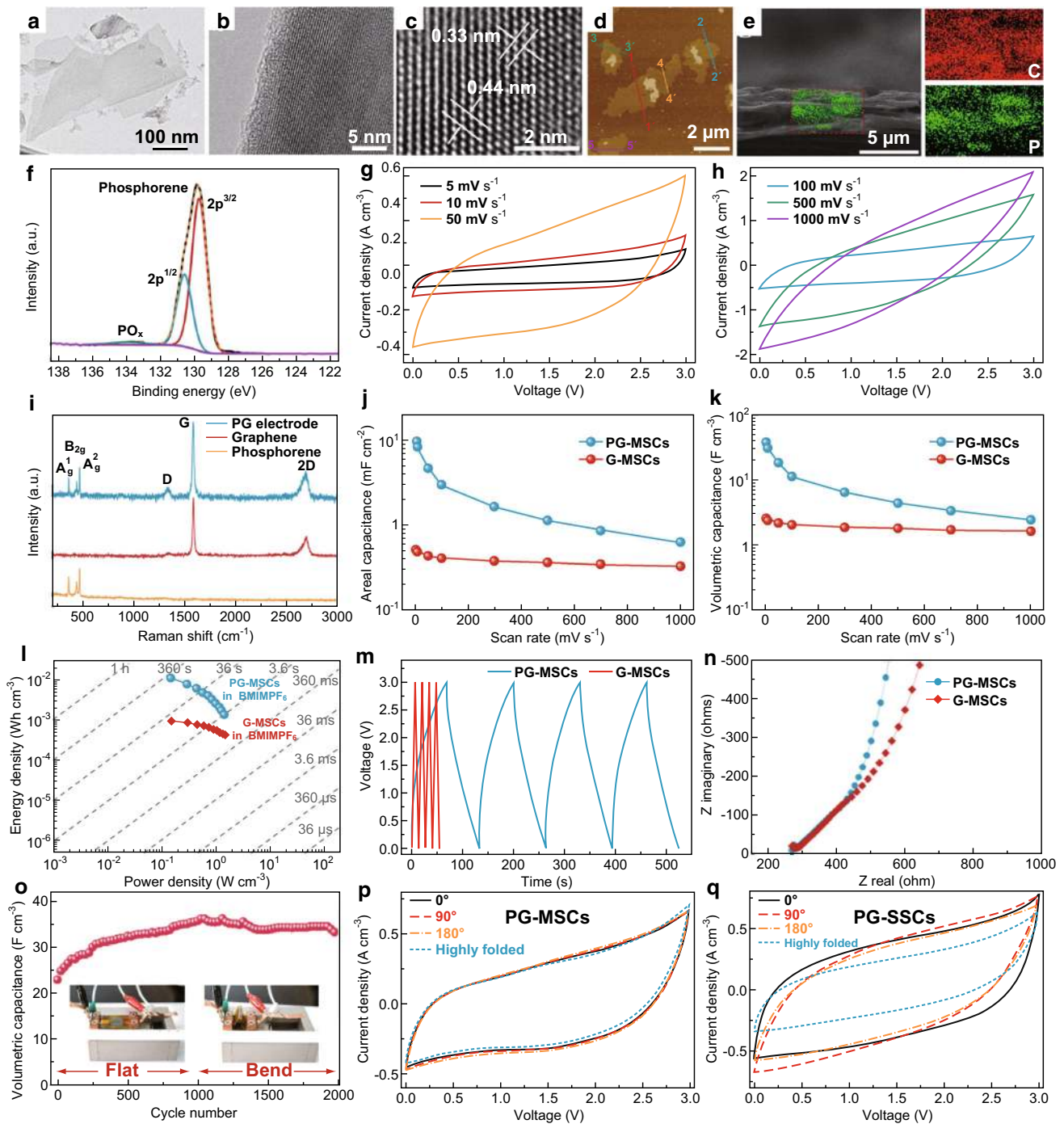
Fig. 10 Structural characterization and electrochemical performance analysis of phosphorene as a supercapacitor electrode: **a** TEM image of phosphorene thin film **b** HRTEM image of the phosphorene thin film. **c** HRTEM micrograph of the phosphorene thin film with atomic positions and lattice parameters. **d** AFM image of the phosphorene thin film. **e** SEM image of the cross section of the phosphorene thin film with EDX spectra of the selected region. **f** XPS spectra of phosphorene thin film. **g**, **h** CV at varying scan rates of P/G anode and G anode, respectively. **i** XRD spectra stack of the phosphorene (orange), graphene (red) ,and P/G composite electrode (blue). **j** Aerial capacitances of P/G (blue) and G (red) samples. **k** Volumetric capacitances of P/G (blue) and G (red) samples. **l** Ragone plots of P/G (blue) and G (red) samples. **m** GCD curves of the P/G (blue) and G (red) samples at a current density of 0.3 A cm^{-3}. **n** Complex part of the impedance spectra of P/G (blue) and the G (red) samples. **o** Stability performance of the P/G sample over 2000 cycles with the inset pictures showing the flat and bending orientations. **p** CV curves of the P/G composite micro-supercapacitor. **q** CV curves of the P/G composite on PET substrate [174]. Copyright 2017 American Chemical Society. (Color figure online)

Table 7 Performance of BP/phosphorene electrodes in various non-Li supercapacitor systems

Type of BP/phosphorene	Electrolyte chemistry	Performance*	References
phosphorene/graphene	$BMIMPF_6$	9.8 mF cm^{-2}/0.44 A cm^{-3}	[174]
BP/PANI	1 M H_2SO_4	354 F g^{-1}/0.3 A g^{-1}	[170]
BP nanoflake/CNT	PVA/H_3PO_4	41.4 F cm^{-3}/5 mV s^{-1}	[172]
BP nanosheet/PPy	PVA/H_3PO_4	452.8 F g^{-1}/0.5 A g^{-1}	[173]
BP nanoflake	PVA/H_3PO_4	45.8 F g^{-1}/10 mV s^{-1}	[171]

*Capacitance (areal/volumetric/specific)/current density

As anodes in non-Li metal ion rechargeable systems, *Phosphorene* has been applied relatively sparsely compared to TMDs and MXenes. In this case, the scalability of the fabrication procedure is an important issue. The mechanical cleavage technique used is not suitable for bulk production, although it results in highly pure crystals [182, 183]. To address this challenge, plasma-assisted and liquid phase exfoliation processes have been proposed [183]. Also, a large anisotropic volume expansion ($\sim$ 92% and $\sim$ 160% along the *y* and *z*-directions, respectively) is observed in pure phosphorene due to Na$^+$ ion intercalation, which has been addressed by using it as a nanocomposite with graphene [164].

7 Conclusion

Newer and cleaner energy generation techniques require improved and reliable energy storage systems with viable economics. Non-LIBs, e.g., SIBs, KIBs, MIBs, are seen as increasingly attractive alternative because they can be suitably utilized for large-scale grid storage at a reduced cost compared to LIB systems. However, these systems are faced with their own set of challenges which have not been resolved by utilizing conventional anodes analogous to those used in LIB systems.

It is anticipated that 2D materials, with their layered morphology (and consequently large surface area), high mechanical and chemical stability, and their diverse and tunable electronic properties will be gradually introduced as ideal alternatives once the aforementioned limitations are addressed. Moreover, they are best suited to address the highlighted deficiencies of LIB systems. Phenomenologically, the layered structure of these 2D materials will help in accommodating the large mono- and multivalent alkali metal ions and also provide a large number of electroactive sites for reactions to proceed. All these advantages notwithstanding, 2D materials pose their own problems as well; high cost, volume changes during the intercalation process and difficulty in maintaining the sheet-like morphology, poor reversibility, etc., are some of the issues that need to be thoroughly examined in detail before 2D materials can be widely applied. This multitude of fundamental and experimental hurdles can be overcome using a variety of approaches such as the addition of intercalants/dopants to enhance interstitial spacing, the synthesis of composite electrodes to enhance strength, and the manipulation of surface properties via surface functionalization are some of the innovative techniques that are being increasingly exploited to maximize the efficiency of these materials. In addition, these techniques could serve to improve our understanding of the overall electrochemical mechanisms involved, which may provide better insight into efficacious electrode designs which would facilitate the effective exploitation of the capabilities of 2D materials.

References

1. N. Nitta, F. Wu, J.T. Lee, G. Yushin, Li-ion battery materials: present and future. Mater. Today **18**(5), 252–264 (2015). https://doi.org/10.1016/j.mattod.2014.10.040

2. V. Etacheri, R. Marom, R. Elazari, G. Salitra, D. Aurbach, Challenges in the development of advanced li-ion batteries: a review. Energy Environ. Sci. **4**, 3243–3262 (2011). https://doi.org/10.1039/C1EE01598B

3. X. Xie, S. Wang, K. Kretschmer, G. Wang, Two-dimensional layered compound based anode materials for lithium-ion batteries and sodium-ion batteries. J. Colloid Interface Sci. **499**, 17–32 (2017). https://doi.org/10.1016/j.jcis.2017.03.077

4. R.D. Shannon, Revised effective ionic radii and systematic studies of interatomic distances in halides and chalcogenides. Acta Crystallogr. A **32**, 751–767 (1976). https://doi.org/10.1107/s0567739476001551

5. L. Peng, Y. Zhu, D. Chen, R.S. Ruoff, G. Yu, Two-dimensional materials for beyond-lithium-ion batteries. Adv. Energy Mater. **6**, 1600025–1600045 (2016). https://doi.org/10.1002/aenm.201600025

6. B. Scrosati, J. Hassoun, Y.-K. Sun, Lithium-ion batteries, A look into the future. Energy Environ. Sci. **4**, 3287–3295 (2011). https://doi.org/10.1039/C1EE01388B

7. T. Ichitsubo, T. Adachi, S. Yagi, T. Doi, Potential positive electrodes for high-voltage magnesium-ion batteries. J. Mater. Chem. **21**, 11764–11772 (2011). https://doi.org/10.1039/C1JM11793A

8. M.D. Slater, D. Kim, E. Lee, C.S. Johnson, Sodium-ion batteries. Adv. Funct. Mater. **23**, 947–958 (2013)

9. Y. Wang, R. Chen, T. Chen, H. Lv, G. Zhu, L. Ma, C. Wang, Z. Jin, J. Liu, Emerging non-lithium ion batteries. Energy Storage Mater. **4**, 103–129 (2016). https://doi.org/10.1016/j.ensm.2016.04.001

10. Y. Chen, W. Luo, M. Carter, L. Zhou, J. Dai et al., Organic electrode for non-aqueous potassium-ion batteries. Nano Energy **18**, 205–211 (2015). https://doi.org/10.1016/j.nanoen.2015.10.015

11. Y. Zhou, Y. Yang, M. Jiao, Z. Zhou, What is the promising anode material for Na ion batteries? Sci. Bull. **63**, 146–148 (2018). https://doi.org/10.1016/j.scib.2018.01.011

12. D.R.S. Few, O. Schmidt, A. Gambhir, *Electrical Energy Storage for Mitigating Climate Change*, Briefing Paper No 20 (Grantham Institute, Imperial College, London, UK, 2016), pp. 1–23. https://hdl.handle.net/10044/1/37495

13. Y. Han, Y. Ge, Y. Chao, C. Wang, G.G. Wallace, Recent progress in 2d materials for flexible supercapacitors. J. Energy Chem. **27**, 57–72 (2018). https://doi.org/10.1016/j.jechem.2017.10.033

14. M.J. Allen, V.C. Tung, R.B. Kaner, Honeycomb carbon: a review of graphene. Chem. Rev. **110**, 132–145 (2010). https://doi.org/10.1021/cr900070d

15. Y. Jing, Z. Zhou, C.R. Cabrera, Z. Chen, Graphene, inorganic graphene analogs and their composites for lithium ion batteries. J. Mater. Chem. A **2**, 12104–12122 (2014). https://doi.org/10.1039/C4TA01033G

16. A. Peigney, C. Laurent, E. Flahaut, R.R. Bacsa, A. Rousset, Specific surface area of carbon nanotubes and bundles of carbon nanotubes. Carbon **39**, 507–514 (2001). https://doi.org/10.1016/S0008-6223(00)00155-X

17. C. Lee, X. Wei, J.W. Kysar, J. Hone, Measurement of the elastic properties and intrinsic strength of monolayer graphene. Science **321**, 385–388 (2008). https://doi.org/10.1126/science.1157996

18. X. Yu, H. Cheng, M. Zhang, Y. Zhao, L. Qu, G. Shi, Graphene-based smart materials. Nat. Rev. Mater. **2**, 17046 (2017). https://doi.org/10.1038/natrevmats.2017.46

19. M. Pumera, Z. Sofer, A. Ambrosi, Layered transition metal dichalcogenides for electrochemical energy generation and storage. J. Mater. Chem. A **2**, 8981–8987 (2014). https://doi.org/10.1039/C4TA00652F

20. M. Donarelli, S. Prezioso, F. Perrozzi, F. Bisti, M. Nardone, L. Giancaterini, C. Cantalini, L. Ottaviano, Response to NO_2 and other gases of resistive chemically exfoliated MoS_2-based gas sensors. Sensor Actuat. B: Chem. **207**, 602–613 (2015). https://doi.org/10.1016/j.snb.2014.10.099

21. J.-C. Lei, X. Zhang, Z. Zhou, Recent advances in MXene: preparation, properties, and applications. Front. Phys. **10**, 276–286 (2015). https://doi.org/10.1007/s11467-015-0493-x

22. B. Anasori, Y. Xie, M. Beidaghi, J. Lu, B.C. Hosler, L. Hultman, P.R.C. Kent, Y. Gogotsi, M.W. Barsoum, Two-dimensional, ordered, double transition metals carbides (MXenes). ACS Nano **9**, 9507–9516 (2015). https://doi.org/10.1021/acsnano.5b03591

23. Q. Hu, D. Sun, Q. Wu, H. Wang, L. Wang, B. Liu, A. Zhou, J. He, MXene: a new family of promising hydrogen storage medium. J. Phys. Chem. A **117**, 14253–14260 (2013). https://doi.org/10.1021/jp409585v

24. H. Liu, A.T. Neal, Z. Zhu, Z. Luo, X. Xu, D. Tomanek, P.D. Ye, Phosphorene: an unexplored 2d semiconductor with a high hole mobility. ACS Nano **8**, 4033–4041 (2014). https://doi.org/10.1021/nn501226z

25. S. Zhao, W. Kang, J. Xue, The potential application of phosphorene as an anode material in Li-ion batteries. J. Mater. Chem. A **2**, 19046–19052 (2014). https://doi.org/10.1039/C4TA04368E

26. A. Sibari, A.E. Marjaoui, M. Lakhal, Z. Kerrami, A. Kara et al., Phosphorene as a promising anode material for (Li/Na/Mg)-ion batteries: a first-principle study. Sol. Energy Mater. Sol. Cells **180**, 253–257 (2018). https://doi.org/10.1016/j.solmat.2017.06.034

27. J. Dai, X.C. Zeng, Bilayer phosphorene: effect of stacking order on bandgap and its potential applications in thin-film solar cells. J. Phys. Chem. Lett. **5**, 1289–1293 (2014). https://doi.org/10.1021/jz500409m

28. L. Kou, T. Frauenheim, C. Chen, Phosphorene as a superior gas sensor: selective adsorption and distinct i–v response. J. Phys. Chem. Lett. **5**, 2675–2681 (2014). https://doi.org/10.1021/jz501188k

29. R. Raccichini, A. Varzi, S. Passerini, B. Scrosati, The role of graphene for electrochemical energy storage. Nat. Mater. **14**, 271–279 (2015). https://doi.org/10.1038/nmat4170

30. W. Lv, Z. Li, Y. Deng, Q.-H. Yang, F. Kang, Graphene-based materials for electrochemical energy storage devices: opportunities and challenges. Energy Storage Mater. **2**, 107–138 (2016). https://doi.org/10.1016/j.ensm.2015.10.002

31. Z. Jian, W. Luo, X. Ji, Carbon electrodes for k-ion batteries. J. Am. Chem. Soc. **137**, 11566–11569 (2015). https://doi.org/10.1021/jacs.5b06809

32. S. Chen, C. Wu, L. Shen, C. Zhu, Y. Huang, K. Xi, J. Maier, Y. Yu, Challenges and perspectives for nasicon-type electrode materials for advanced sodium-ion batteries. Adv. Mater. (2017). https://doi.org/10.1002/adma.201700431

33. I. Sultana, M.M. Rahman, S. Mateti, V.G. Ahmadabadi, A.M. Glushenkov, Y. Chen, K-ion and Na-ion storage performances of CO_3O_4–Fe_2O_3 nanoparticle-decorated super p carbon black prepared by a ball milling process. Nanoscale **9**, 3646–3654 (2017). https://doi.org/10.1039/C6NR09613A

34. N. Wu, Y.-C. Lyu, R.-J. Xiao, X. Yu, Y.-X. Yin, X.-Q. Yang, H. Li, L. Gu, Y.-G. Guo, A highly reversible, low-strain Mg-ion insertion anode material for rechargeable mg-ion batteries. NPG Asia Mater. **6**, e120 (2014). https://doi.org/10.1038/am.2014.61

35. X. Fan, J. Mao, Y. Zhu, C. Luo, L. Suo, T. Gao, F. Han, S.C. Liou, C. Wang, Superior stable self-healing SnP_3 anode for sodium-ion batteries. Adv. Energy Mater. **5**, 1500174 (2015). https://doi.org/10.1002/aenm.201500174

36. W. Zhang, J. Mao, S. Li, Z. Chen, Z. Guo, Phosphorus-based alloy materials for advanced potassium-ion battery anode. J. Am. Chem. Soc. **139**, 3316–3319 (2017). https://doi.org/10.1021/jacs.6b12185

37. H.D. Yoo, I. Shterenberg, Y. Gofer, G. Gershinsky, N. Pour, D. Aurbach, Mg rechargeable batteries: an on-going challenge. Energy Environ. Sci. **6**, 2265–2279 (2013). https://doi.org/10.1039/c3ee40871j

38. L. Shi, T. Zhao, Recent advances in inorganic 2d materials and their applications in lithium and sodium batteries. J. Mater. Chem. A **5**, 3735–3758 (2017). https://doi.org/10.1039/C6TA09831B

39. P. Kumar, H. Abuhimd, W. Wahyudi, M. Li, J. Ming, L.-J. Li, Review—two-dimensional layered materials for energy storage applications. ECS J. Solid State Sci. Technol. **5**, Q3021–Q3025 (2016). https://doi.org/10.1149/2.0051611jss

40. L. Kou, C. Chen, S.C. Smith, Phosphorene: fabrication, properties, and applications. J. Phys. Chem. Lett. **6**, 2794–2805 (2015). https://doi.org/10.1021/acs.jpclett.5b01094

41. M. Chhowalla, H.S. Shin, G. Eda, L.-J. Li, K.P. Loh, H. Zhang, The chemistry of two-dimensional layered transition metal dichalcogenide nanosheets. Nat. Chem. **5**, 263–275 (2013). https://doi.org/10.1038/nchem.1589

42. J.A. Wilson, A.D. Yoffe, The transition metal dichalcogenides discussion and interpretation of the observed optical, electrical and structural properties. Adv. Phys. **18**, 193–335 (1969). https://doi.org/10.1080/00018736900101307

43. Y.C. Jiang, J. Gao, L. Wang, Raman fingerprint for semi-metal WTe_2 evolving from bulk to monolayer. Sci. Rep. **6**, 19624 (2016). https://doi.org/10.1038/srep19624

44. J.A. Wilson, F.J.D. Salvo, S. Mahajan, Charge-density waves and superlattices in the metallic layered transition metal dichalcogenides. Adv. Phys. **24**, 117–201 (1975). https://doi.org/10.1080/00018737500101391

45. A.K. Geim, K.S. Novoselov, The rise of graphene. Nat. Mater. **6**, 183–191 (2007). https://doi.org/10.1038/nmat1849

46. S. Bertolazzi, J. Brivio, A. Kis, Stretching and breaking of ultrathin MoS_2. ACS Nano **5**, 9703–9709 (2011). https://doi.org/10.1021/nn203879f

47. X. Huang, Z. Zeng, H. Zhang, Metal dichalcogenide nanosheets: preparation, properties and applications. Chem. Soc. Rev. **42**, 1934–1946 (2013). https://doi.org/10.1039/c2cs35387c

48. B. Anasori, M.R. Lukatskaya, Y. Gogotsi, 2d metal carbides and nitrides (MXenes) for energy storage. Nat. Rev. Mater. **2**, 16098 (2017). https://doi.org/10.1038/natrevmats.2016.98

49. M. Naguib, V.N. Mochalin, M.W. Barsoum, Y. Gogotsi, Mxenes: a new family of two-dimensional materials. Adv. Mater. **26**, 992–1005 (2014). https://doi.org/10.1002/adma.201304138

50. M.W. Barsoum, M. Radovic, Elastic and mechanical properties of the max phases. Ann. Rev. Mater. Res. **41**, 195–227 (2011). https://doi.org/10.1146/annurev-matsci-062910-100448

51. Q. Tang, Z. Zhou, P. Shen, Are MXenes promising anode materials for li ion batteries? Computational studies on electronic properties and li storage capability of Ti_3C_2 and $Ti_3C_2X_2$ (X = F, OH) monolayer. J. Am. Chem. Soc. **134**, 16909–16916 (2012). https://doi.org/10.1021/ja308463r

52. M. Naguib, R.R. Unocic, B.L. Armstrong, J. Nanda, Large-scale delamination of multi-layers transition metal carbides and carbonitrides "MXenes". Dalton Trans. **44**, 9353–9358 (2015). https://doi.org/10.1039/C5DT01247C

53. H.W. Wang, M. Naguib, K. Page, D.J. Wesolowski, Y. Gogotsi, Resolving the structure of $Ti_3C_2T_x$ MXenes through multi-level structural modeling of the atomic pair distribution function. Chem. Mat. **28**, 349–359 (2015). https://doi.org/10.1021/acs.chemmater.5b04250

54. Q. Wei, X. Peng, Superior mechanical flexibility of phosphorene and few-layer black phosphorus. Appl. Phys. Lett. **104**, 251915 (2014). https://doi.org/10.1063/1.4885215

55. A. Khandelwal, K. Mani, M.H. Karigerasi, I. Lahiri, Phosphorene – the two-dimensional black phosphorous: properties, synthesis and applications. Mater. Sci. Eng. B **221**, 17–34 (2017). https://doi.org/10.1016/j.mseb.2017.03.011

56. A. Castellanos-Gomez, Black phosphorus: narrow gap, wide applications. J. Phys. Chem. Lett. **6**, 4280–4291 (2015). https://doi.org/10.1021/acs.jpclett.5b01686

57. H.Y. Lv, W.J. Lu, D.F. Shao, Y.P. Sun, Enhanced thermoelectric performance of phosphorene by strain-induced band convergence. Phys. Rev. B **90**, 085433 (2014). https://doi.org/10.1103/PhysRevB.90.085433

58. L. Zhu, G. Zhang, B. Li, Coexistence of size-dependent and size-independent thermal conductivities in phosphorene. Phys. Rev. B **90**, 214302 (2014). https://doi.org/10.1103/PhysRevB.90.214302

59. Y.-Y. Zhang, Q.-X. Pei, J.-W. Jiang, N. Wei, Y.-W. Zhang, Thermal conductivities of single- and multi-layer phosphorene: a molecular dynamics study. Nanoscale **8**, 483–491 (2016). https://doi.org/10.1039/C5NR05451F

60. Y. Jing, X. Zhang, Z. Zhou, Phosphorene: what can we know from computations? WIREs Comput. Mol. Sci. **6**, 5–19 (2016). https://doi.org/10.1002/wcms.1234

61. P. Srivastava, K.P.S.S. Hembram, H. Mizuseki, K.R. Lee, S.S. Han, S. Kim, Tuning the electronic and magnetic properties of phosphorene by vacancies and adatoms. J. Phys. Chem. C **119**, 6530–6538 (2015). https://doi.org/10.1021/jp5110938

62. S. Pan, J. He, C. Wang, Y. Zuo, Exfoliation of two-dimensional phosphorene sheets with enhanced photocatalytic activity under simulated sunlight. Mater. Lett. **212**, 311–314 (2018). https://doi.org/10.1016/j.matlet.2017.10.090

63. H. Kaur, S. Yadav, A.K. Srivastava, N. Singh, J.J. Schneider, O.P. Sinha, V.V. Agrawal, R. Srivastava, Large area fabrication of semiconducting phosphorene by langmuir-blodgett assembly. Sci. Rep. **6**, 34095 (2016). https://doi.org/10.1038/srep34095

64. Q.X. Xia, J. Fu, J.M. Yun, R.S. Mane, K.H. Kim, High volumetric energy density annealed-mxene-nickel oxide/mxene asymmetric supercapacitor. RSC Adv. **7**, 11000–11011 (2017). https://doi.org/10.1039/C6RA27880A

65. E. Yang, H. Ji, J. Kim, H. Kim, Y. Jung, Exploring the possibilities of two-dimensional transition metal carbides as anode materials for sodium batteries. Phys. Chem. Chem. Phys. **17**, 5000–5005 (2015). https://doi.org/10.1039/C4CP05140H

66. A. Byeon, M.-Q. Zhao, C.E. Ren, J. Halim, S. Kota, P. Urbankowski, B. Anasori, M.W. Barsoum, Y. Gogotsi, Two-dimensional titanium carbide MXene as a cathode material for hybrid magnesium/lithium-ion batteries. ACS Appl. Mater. Interfaces **9**, 4296–4300 (2017). https://doi.org/10.1021/acsami.6b04198

67. S. Xu, G. Wei, J. Li, Y. Ji, N. Klyui, V. Izotov, W. Han, Binder-free $Ti_3C_2T_x$ mxene electrode film for supercapacitor produced by electrophoretic deposition method. Chem. Eng. J. **317**, 1026–1036 (2017). https://doi.org/10.1016/j.cej.2017.02.144

68. X. Zhou, J. Jiang, T. Ding, J. Zhang, B. Pan, J. Zuoa, Q. Yang, Fast colloidal synthesis of scalable mo-rich hierarchical ultrathin $MoSe_{2-x}$ nanosheets for high performance hydrogen evolution. Nanoscale **6**, 11046–11051 (2014). https://doi.org/10.1039/C4NR02716G

69. H. Zhang, X.-L. Fan, Y. Yang, P. Xiao, Strain engineering the magnetic states of vacancy-doped monolayer $MoSe_2$. J. Alloy. Compd. **635**, 307–313 (2015). https://doi.org/10.1016/j.jallcom.2015.02.141

70. M. Bougouma, A. Batan, B. Guel, T. Segato, J.B. Legma, F. Reniers, M.-P. Delplancke-Ogletree, C. Buess-Herman, T. Doneux, Growth and characterization of large, high quality $MoSe_2$ single crystals. J. Cryst. Growth **363**, 122–127 (2013). https://doi.org/10.1016/j.jcrysgro.2012.10.026

71. J. Xia, X. Huang, L.-Z. Liu, M. Wang, L. Wang et al., CVD synthesis of large-area, highly crystalline $MoSe_2$ atomic layers on diverse substrates and application to photodetectors. Nanoscale **6**, 8949–8955 (2014). https://doi.org/10.1039/C4NR02311K

72. D.A.C. Brownson, D.K. Kampouris, C.E. Banks, Graphene electrochemistry: fundamental concepts through to prominent applications. Chem. Soc. Rev. **41**, 6944–6976 (2012). https://doi.org/10.1039/c2cs35105f

73. H. Chengxue, Y. Zhong, S. Xiufeng, Z. Haibo, 2D materials via liquid exfoliation: a review on fabrication and applications. Sci. Bull. **60**, 1994–2008 (2015). https://doi.org/10.1007/s11434-015-0936-3

74. A.H. Khan, S. Ghosh, B. Pradhan, A. Dalui, L.K. Shrestha, S. Acharya, K. Ariga, Two-dimensional (2d) nanomaterials towards electrochemical nanoarchitectonics in energy-related applications. Bull. Chem. Soc. Jpn. **90**, 627–648 (2017). https://doi.org/10.1246/bcsj.20170043

75. H. Zhang, Ultrathin two-dimensional nanomaterials. ACS Nano **9**, 9451–9469 (2015). https://doi.org/10.1021/acsnano.5b05040

76. K.S. Novoselov, D. Jiang, F. Schedin, T.J. Booth, V.V. Khotkevich, S.V. Morozov, A.K. Geim, Two-dimensional atomic crystals. PNAS, USA **102**, 10451–10453 (2005). https://doi.org/10.1073/pnas.0502848102

77. A. Splendiani, L. Sun, Y. Zhang, T. Li, J. Kim, C.Y. Chim, G. Galli, F. Wang, Emerging photoluminescence in monolayer MoS_2. Nano Lett. **10**, 1271–1275 (2010). https://doi.org/10.1021/nl903868w

78. H. Li, J. Wu, Z. Yin, H. Zhang, Preparation and applications of mechanically exfoliated single-layer and multilayer MoS_2 and WSe_2 nanosheets. Acc. Chem. Res. **47**, 1067–1075 (2014). https://doi.org/10.1021/ar4002312

79. K.S. Novoselov, A.K. Geim, S.V. Morozov, D. Jiang, Y. Zhang, S.V. Dubonos, I.V. Grigorieva, A.A. Firsov, Electric field effect in atomically thin carbon films. Science **306**, 666–669 (2004). https://doi.org/10.1126/science.1102896

80. M.H. Rummeli, C.G. Rocha, F. Ortmann, I. Ibrahim, H. Sevincli, Graphene: piecing it together. Adv. Mater. **23**, 4471–4490 (2011). https://doi.org/10.1002/adma.201101855

81. R. Lv, H. Terrones, A.L. Elías, N. Perea-López, R. Gutiérrez, H.E. Cruz-Silva, L.P. Rajukumar, S. Dresselhaus, M. Mauri-cioTerrones, Two-dimensional transition metal dichalcogenides: clusters, ribbons, sheets and more. Nano Today **10**, 559–592 (2015). https://doi.org/10.1016/j.nantod.2015.07.004

82. J.N. Coleman, M. Lotya, A. O'Neill, S.D. Bergin, P.J. King et al., Two-dimensional nanosheets produced by liquid exfoliation of layered materials. Science **331**, 568–571 (2011). https://doi.org/10.1126/science.1194975

83. L. David, R. Bhandavat, G. Singh, MoS_2/graphene composite paper for sodium-ion battery electrodes. ACS Nano **8**, 1759–1770 (2014). https://doi.org/10.1021/nn406156b

84. S. Haar, M. Bruna, J.X. Lian, F. Tomarchio, Y. Olivier et al., Liquid-phase exfoliation of graphite into single- and few-layer graphene with α-functionalized alkanes. J. Phys. Chem. Lett. **7**, 2714–2721 (2016). https://doi.org/10.1021/acs.jpclett.6b01260

85. E. Benavente, M.A.S. Ana, F. Mendizabal, G. Gonzalez, Intercalation chemistry of molybdenum disulfide. Coord. Chem. Rev. **224**, 87–109 (2002). https://doi.org/10.1016/S0010-8545(01)00392-7

86. A.S. Golub, Y.V. Zubavichus, Y.L. Slovokhotov, Y.N. Novikov, Single layer dispersion of transition metal dichalcogenides in the synthesis of intercalation compounds. Russ. Chem. Rev. **72**, 123–141 (2003). https://doi.org/10.1070/RC2003v072n02ABEH000789

87. J. Halim, M.R. Lukatskaya, K.M. Cook, J. Lu, C.R. Smith et al., Transparent conductive two-dimensional titanium carbide epitaxial thin films. Chem. Mat. **26**, 2374–2381 (2014). https://doi.org/10.1021/cm500641a

88. M. Ghidiu, J. Halim, S. Kota, D. Bish, Y. Gogotsi, M.W. Barsoum, Ion-exchange and cation solvation reactions in Ti_3C_2 mxene. Chem. Mat. **28**, 3507–3514 (2016). https://doi.org/10.1021/acs.chemmater.6b01275

89. C.N.R. Rao, H.S.S.R. Matte, U. Maitra, Graphene analogues of inorganic layered materials. Angew. Chem. Intern. Edit. **52**, 13162–13185 (2013). https://doi.org/10.1002/anie.201301548

90. R.A. Vilá, K. Momeni, Q. Wang, B.M. Bersch, N. Lu, M.J. Kim, L.Q. Chen, J.A. Robinson, Bottom-up synthesis of vertically oriented two-dimensional materials. 2D Mater **3**, 041003 (2016). https://doi.org/10.1088/2053-1583/3/4/041003

91. A. Özden, F. Ay, C. Sevik, N.K. Perkgöz, CVD growth of monolayer MoS_2: role of growth zone configuration and precursors ratio. Jpn. J. Appl. Phys. **56**, 06GG05 (2017). https://doi.org/10.7567/JJAP.56.06GG05

92. J. Yu, J. Li, W. Zhang, H. Chang, Synthesis of high quality two-dimensional materials via chemical vapor deposition. Chem. Sci. **6**, 6705–6716 (2015). https://doi.org/10.1039/C5SC01941A

93. A. Valdivia, D.J. Tweet, Jr. JFC, Atomic layer deposition of two dimensional MoS_2 on 150 mm substrates. J. Vac. Sci. Technol. A **34**, 021515 (2016). https://doi.org/10.1116/1.4941245

94. X. Zhang, Z. Zhang, Z. Zhou, Mxene-based materials for electrochemical energy storage. J. Energy Chem. **27**, 73–85 (2018). https://doi.org/10.1016/j.jechem.2017.08.004

95. D. Geng, X. Zhao, Z. Chen, W. Sun, W. Fu, J. Chen, W. Liu, W. Zhou, K.P. Loh, Direct synthesis of large-area 2D Mo_2C on in situ grown graphene. Adv. Mater. **29**, 1700072 (2017). https://doi.org/10.1002/adma.201700072

96. H. Ye, J. Zhou, D. Er, C.C. Price, Z. Yu, Y. Liu, J. Lowengrub, J. Lou, Z. Liu, V.B. Shenoy, Toward a mechanistic understanding of vertical growth of van der waals stacked 2D materials: a multiscale model and experiments. ACS Nano **11**, 12780–12788 (2017). https://doi.org/10.1021/acsnano.7b07604

97. J. Cai, P. Ruffieux, R. Jaafar, M. Bieri, T. Braun et al., Atomically precise bottom-up fabrication of graphene nanoribbons. Nature **466**, 470–473 (2010). https://doi.org/10.1038/nature09211

98. S. Wu, Y. Du, S. Sun, Transition metal dichalcogenide based nanomaterials for rechargeable batteries. Chem. Eng. J. **307**, 189–207 (2017). https://doi.org/10.1016/j.cej.2016.08.044

99. R. Bhandavat, L. David, G. Singh, Synthesis of surface-functionalized WS_2 nanosheets and performance as li-ion battery anodes. J. Phys. Chem. Lett. **3**, 1523–1530 (2012). https://doi.org/10.1021/jz300480w

100. W. Choi, N. Choudhary, G.H. Han, J. Park, D. Akinwande, Y.H. Lee, Recent development of two-dimensional transition metal dichalcogenides and their applications. Mater. Today **20**, 116–130 (2017). https://doi.org/10.1016/j.mattod.2016.10.002

101. Y. Yang, H. Fei, G. Ruan, C. Xiang, J.M. Tour, Edge-oriented MoS_2 nanoporous films as flexible electrodes for hydrogen evolution reactions and supercapacitor devices. Adv. Mater. **26**, 8163–8168 (2014). https://doi.org/10.1002/adma.201402847

102. M. Acerce, D. Voiry, M. Chhowalla, Metallic 1t phase MoS_2 nanosheets as supercapacitor electrode materials. Nat. Nanotechnol. **10**, 313–318 (2015). https://doi.org/10.1038/nnano.2015.40

103. F. Li, Z. Zhou, Micro/nanostructured materials for sodium ion batteries and capacitors. Small **14**, 1702961–1702986 (2018). https://doi.org/10.1002/smll.201702961

104. M. Mortazavi, C. Wang, J. Deng, V.B. Shenoy, N.V. Medhekar, Ab initio characterization of layered MoS_2 as anode for sodium-ion batteries. J. Power Sources **268**, 279–286 (2014). https://doi.org/10.1016/j.jpowsour.2014.06.049

105. H. Chen, Q. Ha, O. Zivkovic, G. Hautier, L.-S. Du et al., Sidorenkite ($Na_3MnPO_4CO_3$): a new intercalation cathode material for na-ion batteries. Chem. Mat. **25**, 2777–2786 (2013). https://doi.org/10.1021/cm400805q

106. Q. Li, Z. Yao, J. Wu, S. Mitra, S. Hao, T.S. Sahu, Y. Li, C. Wolverton, V.P. Dravid, Intermediate phases in sodium intercalation into MoS_2 nanosheets and their implications for sodium-ion batteries. Nano Energy **38**, 342–349 (2017). https://doi.org/10.1016/j.nanoen.2017.05.055

107. D.W. Su, S.X. Dou, G.X. Wang, Ultrathin MoS_2 nanosheets as anode materials for sodium-ion batteries with superior performance. Adv. Energy Mater. **5**, 1401205 (2015). https://doi.org/10.1002/aenm.201401205

108. G.S. Bang, K.W. Nam, J.Y. Kim, J. Shin, J.W. Choi, S.-Y. Choi, Effective liquid-phase exfoliation and sodium ion battery application of MoS_2 nanosheets. ACS Appl. Mater. Interfaces **6**, 7084–7089 (2014). https://doi.org/10.1021/am4060222

109. S.D. Lacey, J. Wan, W.C.A. Von, S.M. Russell, J. Dai, W. Bao, K. Xu, L. Hu, Atomic force microscopy studies on molybdenum disulfide flakes as sodium-ion anodes. Nano Lett. **15**, 1018–1024 (2015). https://doi.org/10.1021/nl503871s

110. K. Share, J. Lewis, L. Oakes, R.E. Carter, A.P. Cohn, C.L. Pint, Tungsten diselenide (WSe$_2$) as a high capacity, low overpotential conversion electrode for sodium ion batteries. RSC Adv. **5**, 101262–101267 (2015). https://doi.org/10.1039/C5RA19717A

111. M. Li, Z. Wu, Z. Wang, S. Yu, Y. Zhu, B. Nan, Y. Shi, Facile synthesis of ultrathin MoS$_2$/C nanosheets for use in sodium-ion batteries. RSC Adv. **7**, 285–289 (2017). https://doi.org/10.1039/C6RA24800D

112. S. Zhang, X. Yu, H. Yu, Y. Chen, P. Gao, C. Li, C. Zhu, Growth of ultrathin MoS$_2$ nanosheets with expanded spacing of (002) plane on carbon nanotubes for high-performance sodium-ion battery anodes. ACS Appl. Mater. Interfaces **6**, 21880–21885 (2014). https://doi.org/10.1021/am5061036

113. Y. Liu, X. He, D. Hanlon, A. Harvey, J.N. Coleman, Y. Li, Liquid phase exfoliated MoS$_2$ nanosheets percolated with carbon nanotubes for high volumetric/areal capacity sodium-ion batteries. ACS Nano **10**, 8821–8828 (2016). https://doi.org/10.1021/acsnano.6b04577

114. Z. Zhang, X. Yang, Y. Fu, K. Du, Ultrathin molybdenum diselenide nanosheets anchored on multi-walled carbon nanotubes as anode composites for high performance sodium-ion batteries. J. Power Sources **296**, 2–9 (2015). https://doi.org/10.1016/j.jpowsour.2015.07.008

115. Y. Zhang, Z. Liu, H. Zhao, Y. Du, MoSe$_2$ nanosheets grown on carbon cloth with superior electrochemical performance as flexible electrode for sodium ion batteries. RSC Adv. **6**, 1440–1444 (2016). https://doi.org/10.1039/C5RA24852C

116. F. Niu, J. Yang, N. Wang, D. Zhang, W. Fan, J. Yang, Y. Qian, MoSe$_2$-covered n, p-doped carbon nanosheets as a long-life and high-rate anode material for sodium-ion batteries. Adv. Funct. Mater. **27**, 170052 (2017). https://doi.org/10.1002/adfm.201700522

117. K. Xie, K. Yuan, X. Li, W. Lu, C. Shen, C. Liang, Superior potassium ion storage via vertical MoS$_2$ "nano-rose" with expanded interlayers on graphene. Small **13**, 1701471 (2017). https://doi.org/10.1002/smll.201701471

118. B. Liu, T. Luo, G. Mu, X. Wang, D. Chen, G. Shen, Rechargeable Mg-ion batteries based on WSe$_2$ nanowire cathodes. ACS Nano **7**, 8051–8058 (2013). https://doi.org/10.1021/nn4032454

119. S.-K. Park, J. Lee, S. Bong, B. Jang, K.-D. Seong, Y. Piao, Scalable synthesis of few-layer MoS$_2$ incorporated into hierarchical porous carbon nanosheets for high-performance Li and Na battery anodes. ACS Appl. Mater. Interfaces **8**, 19456–19465 (2016). https://doi.org/10.1021/acsami.6b05010

120. Y. Liang, H.D. Yoo, Y. Li, J. Shuai, H.A. Calderon, F.C.R. Hernandez, L.C. Grabow, Y. Yao, Interlayer-expanded molybdenum disulfide nanocomposites for electrochemical magnesium storage. Nano Lett. **15**, 2194–2202 (2015). https://doi.org/10.1021/acs.nanolett.5b00388

121. H. Wang, X. Lan, D. Jiang, Y. Zhang, H. Zhong, Z. Zhanga, Y. Jiang, Sodium storage and transport properties in pyrolysis synthesized MoSe$_2$ nanoplates for high performance sodium-ion batteries. J. Power Sources **283**, 187–194 (2015). https://doi.org/10.1016/j.jpowsour.2015.02.096

122. Z. Zhang, X. Yang, Y. Fu, Nanostructured WSe$_2$/C composites as anode materials for sodium-ion batteries. RSC Adv. **6**, 12726–12729 (2016). https://doi.org/10.1039/C5RA25645C

123. X. Ren, Q. Zhao, W.D. McCulloch, Y. Wu, MoS$_2$ as a long-life host material for potassium ion intercalation. Nano Res. **10**, 1313–1321 (2017). https://doi.org/10.1007/s12274-016-1419-9

124. Y. Liu, L. Jiao, Q. Wu, Y. Zhao, K. Cao, H. Liu, Y. Wang, H. Yuan, Synthesis of rgo-supported layered MoS$_2$ for high-performance rechargeable Mg batteries. Nanoscale **5**, 9562–9567 (2013). https://doi.org/10.1039/c3nr02850j

125. E.G.D.S. Firmiano, A.C. Rabelo, C.J. Dalmaschio, A.N. Pinheiro, E.C. Pereira, W.H. Schreiner, E.R. Leite, Supercapacitor electrodes obtained by directly bonding 2d MoS$_2$ on reduced graphene oxide. Adv. Energy Mater. **4**, 1301380 (2014). https://doi.org/10.1002/aenm.201301380

126. K.-J. Huang, L. Wang, Y.-J. Liu, Y.-M. Liu, H.B. Wang, T. Gan, L.-L. Wang, Layered MoS$_2$–graphene composites for supercapacitor applications with enhanced capacitive performance. Int. J. Hydrogen Energy **38**, 14027–14034 (2013). https://doi.org/10.1016/j.ijhydene.2013.08.112

127. J. Wang, Z. Wu, K. Hu, X. Chen, H. Yin, High conductivity graphene-like MoS$_2$/polyaniline nanocomposites and its application in supercapacitor. J. Alloy. Compd. **619**, 38–43 (2015). https://doi.org/10.1016/j.jallcom.2014.09.008

128. L. Cao, S. Yang, W. Gao, Z. Liu, Y. Gong et al., Direct laser-patterned micro-supercapacitors from paintable MoS$_2$ films. Small **9**, 2905–2910 (2013). https://doi.org/10.1002/smll.201203164

129. S.K. Balasingam, J.S. Lee, Y. Jun, Few-layered MoSe$_2$ nanosheets as an advanced electrode material for supercapacitors. Dalton Trans. **44**, 15491–15498 (2015). https://doi.org/10.1039/C5DT01985K

130. K.-J. Huang, J.-Z. Zhang, Y. Fan, Preparation of layered MoSe$_2$ nanosheets on Ni-foam substrate with enhanced supercapacitor performance. Mater. Lett. **152**, 244–247 (2015). https://doi.org/10.1016/j.matlet.2015.03.130

131. K.-J. Huang, J.-Z. Zhang, J.-L. Cai, Preparation of porous layered molybdenum selenide-graphene composites on Ni foam for high-performance supercapacitor and electrochemical sensing. Electrochim. Acta **180**, 770–777 (2015). https://doi.org/10.1016/j.electacta.2015.09.016

132. C.C. Mayorga-Martinez, A. Ambrosi, A.Y.S. Eng, Z. Sofer, M. Pumera, Transition metal dichalcogenides (MoS$_2$, MoSe2, WS$_2$ and WSe$_2$) exfoliation technique has strong influence upon their capacitance. Electrochem. Commun. **56**, 24–28 (2015). https://doi.org/10.1016/j.elecom.2015.03.017

133. S. Ratha, C.S. Rout, Supercapacitor electrodes based on layered tungsten disulfide-reduced graphene oxide hybrids synthesized by a facile hydrothermal method. ACS Appl. Mater. Interfaces **5**, 11427–11433 (2013). https://doi.org/10.1021/am403663f

134. C. Eames, M.S. Islam, Ion intercalation into two-dimensional transition-metal carbides: global screening for new high-capacity battery materials. J. Am. Chem. Soc. **136**, 16270–16276 (2014). https://doi.org/10.1021/ja508154e

135. Y. Xie, Y. Dall'Agnese, M. Naguib, Y. Gogotsi, M.W. Barsoum, H.L. Zhuang, P.R.C. Kent, Prediction and characterization of MXene nanosheet anodes for non-lithium-ion batteries. ACS Nano **8**, 9606–9615 (2014). https://doi.org/10.1021/nn503921j

136. J. Luo, X. Tao, J. Zhang, Y. Xia, H. Huang, L. Zhang, Y. Gan, C. Liang, W. Zhang, Sn4+ ion decorated highly conductive Ti$_3$C$_2$ mxene: promising lithium-ion anodes with enhanced volumetric capacity and cyclic performance. ACS Nano **10**, 2491–2499 (2016). https://doi.org/10.1021/acsnano.5b07333

137. D. Er, J. Li, M. Naguib, Y. Gogotsi, V.B. Shenoy, Ti$_3$C$_2$ mxene as a high capacity electrode material for metal (Li, Na, K, Ca) ion batteries. ACS Appl. Mater. Interfaces **6**, 11173–11179 (2014). https://doi.org/10.1021/am501144q

138. Q. Sun, Y. Dai, Y. Ma, T. Jing, W. Wei, B. Huang, Ab initio prediction and characterization of Mo$_2$C monolayer as anodes for lithium-ion and sodium-ion batteries. J. Phys. Chem. Lett. **7**, 937–943 (2016). https://doi.org/10.1021/acs.jpclett.6b00171

139. M. Naguib, R.A. Adams, Y. Zhao, D. Zemlyanov, A. Varma, J. Nanda, V.G. Pol, Electrochemical performance of Mxenes as k-ion battery anodes. Chem. Commun. 53, 6883–6886 (2017). https://doi.org/10.1039/C7CC02026K

140. V. Natu, M. Clites, E. Pomerantseva, M.W. Barsoum, Mesoporous mxene powders synthesized by acid induced crumpling and their use as na-ion battery anodes. Mater. Res. Lett. 6, 230–235 (2018). https://doi.org/10.1080/21663831.2018.1434249

141. Y. Wu, P. Nie, L. Wu, H. Dou, X. Zhang, 2d MXene/SnS$_2$ composites as high-performance anodes for sodium ion batteries. Chem. Eng. J. 334, 932–938 (2018). https://doi.org/10.1016/j.cej.2017.10.007

142. Y. Wu, P. Nie, J. Jiang, B. Ding, H. Dou, X. Zhang, Mos$_2$-nanosheet-decorated 2d titanium carbide (MXene) as high-performance anodes for sodium-ion batteries. ChemElectroChem 4, 1560–1565 (2017). https://doi.org/10.1002/celc.201700060

143. X. Guo, X. Xie, S. Choi, Y. Zhao, H. Liu, C. Wang, S. Chang, G. Wang, Sb$_2$O$_3$/mxene(Ti$_3$C$_2$T$_x$) hybrid anode materials with enhanced performance for sodium-ion batteries. J. Mater. Chem. A 5, 12445–12452 (2017). https://doi.org/10.1039/C7TA02689G

144. Y. Dong, Z.-S. Wu, S. Zheng, X. Wang, J. Qin, S. Wang, X. Shi, X. Bao, Ti$_3$C$_2$ MXene-derived sodium/potassium titanate nanoribbons for high-performance sodium/potassium ion batteries with enhanced capacities. ACS Nano 11, 4792–4800 (2017). https://doi.org/10.1021/acsnano.7b01165

145. P. Lian, Y. Dong, Z.-S. Wu, S. Zheng, X. Wang et al., Alkalized Ti$_3$C$_2$ MXene nanoribbons with expanded interlayer spacing for high-capacity sodium and potassium ion batteries. Nano Energy 40, 1–8 (2017). https://doi.org/10.1016/j.nanoen.2017.08.002

146. S. Kajiyama, L. Szabova, K. Sodeyama, H. Iinuma, R. Morita, K. Gotoh, Y. Tateyama, M. Okubo, A. Yamada, Sodium-ion intercalation mechanism in mxene nanosheets. ACS Nano 10, 3334–3341 (2016). https://doi.org/10.1021/acsnano.5b06958

147. M. Xu, S. Lei, J. Qi, Q. Dou, L. Liu, Y. Lu, Q. Huang, S. Shi, X. Yan, Opening magnesium storage capability of two-dimensional MXene by intercalation of cationic surfactant. ACS Nano 12, 3733–3740 (2018). https://doi.org/10.1021/acsnano.8b00959

148. X. Xie, M.-Q. Zhao, B. Anasori, K. Maleski, C.E. Ren et al., Porous heterostructured MXene/carbon nanotube composite paper with high volumetric capacity for sodium-based energy storage devices. Nano Energy 26, 513–523 (2016). https://doi.org/10.1016/j.nanoen.2016.06.005

149. Y. Gao, L. Wang, Z. Li, Y. Zhang, B. Xing, C. Zhang, A. Zhou, Electrochemical performance of Ti$_3$C$_2$ supercapacitors in KOH electrolyte. J. Adv. Ceram. 4(2), 130–134 (2015). https://doi.org/10.1007/s40145-015-0143-3

150. Y. Wen, T.E. Rufford, X. Chen, N. Li, M. Lyu, L. Dai, L. Wang, Nitrogen-doped Ti$_3$C$_2$T$_x$ MXene electrodes for high-performance supercapacitors. Nano Energy 38, 368–376 (2017). https://doi.org/10.1016/j.nanoen.2017.06.009

151. Y. Wang, H. Dou, J. Wang, B. Ding, Y. Xu, Z. Chang, X. Hao, Three-dimensional porous MXene/layered double hydroxide composite for high performance supercapacitors. J. Power Sources 327, 221–228 (2016). https://doi.org/10.1016/j.jpowsour.2016.07.062

152. M.-Q. Zhao, C.E. Ren, Z. Ling, M.R. Lukatskaya, C. Zhang, K.L.V. Aken, M.W. Barsoum, Y. Gogotsi, Flexible MXene/carbon nanotube composite paper with high volumetric capacitance. Adv. Mater. 27, 339–345 (2015). https://doi.org/10.1002/adma.201404140

153. J. Yan, C.E. Ren, K. Maleski, C.B. Hatter, B. Anasori, P. Urbankowski, A. Sarycheva, Y. Gogotsi, Flexible MXene/graphene films for ultrafast supercapacitors with outstanding volumetric capacitance. Adv. Func. Mater. 27, 1701264 (2017). https://doi.org/10.1002/adfm.201701264

154. Z. Lin, D. Barbara, P.-L. Taberna, K.L.V. Aken, B. Anasori, Y. Gogotsi, P. Simon, Capacitance of Ti$_3$C$_2$T$_x$ MXene in ionic liquid electrolyte. J. Power Sources 326, 575–579 (2016). https://doi.org/10.1016/j.jpowsour.2016.04.035

155. R.B. Rakhi, B. Ahmed, M.N. Hedhili, D.H. Anjum, H.N. Alshareef, Effect of postetch annealing gas composition on the structural and electrochemical properties of Ti$_2$CT$_x$ MXene electrodes for supercapacitor applications. Chem. Mat. 27, 5314–5323 (2015). https://doi.org/10.1021/acs.chemmater.5b01623

156. S.-Y. Lin, X. Zhang, Two-dimensional titanium carbide electrode with large mass loading for supercapacitor. J. Power Sources 294, 354–359 (2015). https://doi.org/10.1016/j.jpowsour.2015.06.082

157. E.T. Sisakht, F. Fazileh, M.H. Zare, M. Zarenia, F.M. Peeters, Strain-induced topological phase transition in phosphorene and in phosphorene nanoribbons. Phys. Rev. B 94, 085417 (2016). https://doi.org/10.1103/PhysRevB.94.085417

158. G.-C. Guo, D. Wang, X.-L. Wei, Q. Zhang, H. Liu, W.-M. Lau, L.-M. Liu, First-principles study of phosphorene and graphene heterostructure as anode materials for rechargeable Li batteries. J. Phys. Chem. Lett. 6, 5002–5008 (2015). https://doi.org/10.1021/acs.jpclett.5b02513

159. V.V. Kulish, O.I. Malyi, C. Persson, P. Wu, Phosphorene as an anode material for Na-ion batteries: a first-principles study. Phys. Chem. Chem. Phys. 17, 13921–13928 (2015). https://doi.org/10.1039/C5CP01502B

160. X. Sun, Z. Wang, Sodium adsorption and diffusion on monolayer black phosphorus with intrinsic defects. Appl. Surf. Sci. 427, 189–197 (2018). https://doi.org/10.1016/j.apsusc.2017.08.199

161. B. Peng, Y. Xu, K. Liu, X. Wang, F.M. Mulder, High-performance and low-cost sodium-ion anode based on a facile black phosphorus–carbon nanocomposite. ChemElectroChem 4, 2140–2144 (2017). https://doi.org/10.1002/celc.201700345

162. I. Sultana, M.M. Rahman, T. Ramireddy, Y. Chen, A.M. Glushenkov, High capacity potassium-ion battery anodes based on black phosphorus. J. Mater. Chem. A 5, 23506–23512 (2017). https://doi.org/10.1039/C7TA02483E

163. A. Nie, Y. Cheng, S. Ning, T. Foroozan, P. Yasaei et al., Selective ionic transport pathways in phosphorene. Nano Lett. 16, 2240–2247 (2016). https://doi.org/10.1021/acs.nanolett.5b04514

164. J. Sun, H.-W. Lee, M. Pasta, H. Yuan, G. Zheng, Y. Sun, Y. Li, Y. Cui, A phosphorene–graphene hybrid material as a high-capacity anode for sodium-ion batteries. Nat. Nanotechnol. 10, 980–985 (2015). https://doi.org/10.1038/nnano.2015.194

165. C. Chowdhury, S. Karmakar, A. Datta, Capping black phosphorene by h-BN enhances performances in anodes for Li and Na ion batteries. ACS Energy Lett. 1, 253–259 (2016). https://doi.org/10.1021/acsenergylett.6b00164

166. X. Ren, P. Lian, D. Xie, Y. Yang, Y. Mei, X. Huang, Z. Wang, X. Yin, Properties, preparation and application of black phosphorus/phosphorene for energy storage: a review. J. Mater. Sci. 52, 10364–10386 (2017). https://doi.org/10.1007/s10853-017-1194-3

167. M. Dahbi, N. Yabuuchi, M. Fukunishi, K. Kubota, K. Chihara et al., Black phosphorus as a high-capacity, high-capability negative electrode for sodium-ion batteries: investigation of the electrode/electrolyte interface. Chem. Mat. 28, 1625–1635 (2016). https://doi.org/10.1021/acs.chemmater.5b03524

168. L. Wang, Z. Jiang, W. Li, X. Gu, L. Huang, Hybrid phosphorene/graphene nanocomposite as an anode material for Na-ion batteries: a first principles study. J. Phys. D Appl. Phys. 50,

165501–165507 (2017). https://doi.org/10.1088/1361-6463/aa5aaf

169. X. Han, C. Liu, J. Sun, A.D. Sendek, W. Yang, Density functional theory calculations for evaluation of phosphorene as a potential anode material for magnesium batteries. RSC Adv. **8**, 7196–7204 (2018). https://doi.org/10.1039/C7RA12400G

170. A. Sajedi-Moghaddam, C.C. Mayorga-Martinez, Z. Sofer, D. Bousa, E. Saievar-Iranizad, M. Pumera, Black phosphorus nanoflakes/polyaniline hybrid material for high performance pseudocapacitors. J. Phys. Chem. C **121**, 20532–20538 (2017). https://doi.org/10.1021/acs.jpcc.7b06958

171. C. Hao, B. Yang, F. Wen, J. Xiang, L. Li et al., Flexible all-solid-state supercapacitors based on liquid-exfoliated black-phosphorus nanoflakes. Adv. Mater. **28**(16), 3194–3201 (2016). https://doi.org/10.1002/adma.201505730

172. B. Yang, C. Hao, F. Wen, B. Wang, C. Mu et al., Flexible black-phosphorus nanoflake/carbon nanotube composite paper for high-performance all-solid-state supercapacitors. ACS Appl. Mater. Interfaces **9**, 44478–44484 (2017). https://doi.org/10.1021/acsami.7b13572

173. S. Luo, J. Zhao, J. Zou, Z. He, C. Xu, F. Liu, Y. Huang, L. Dong, L. Wang, H. Zhang, Self-standing polypyrrole/black phosphorus laminated film: promising electrode for flexible supercapacitor with enhanced capacitance and cycling stability. ACS Appl. Mater. Interfaces **10**, 3538–3548 (2018). https://doi.org/10.1021/acsami.7b15458

174. H. Xiao, Z.-S. Wu, L. Chen, F. Zhou, S. Zheng, W. Ren, H.-M. Cheng, X. Bao, One-step device fabrication of phosphorene and graphene interdigital micro-supercapacitors with high energy density. ACS Nano **11**, 7284–7292 (2017). https://doi.org/10.1021/acsnano.7b03288

175. G. Liu, W. Jin, N. Xu, Two-dimensional-material membranes: a new family of high-performance separation membranes. Angew. Chem. Intern. Edit. **55**, 13384–13397 (2016). https://doi.org/10.1002/anie.201600438

176. X. Wang, Z. Guan, Y. Li, Z. Wang, L. Chen, Guest-host interactions and their impacts on structure and performance of Nano-MoS$_2$. Nanoscale **7**, 637–641 (2015). https://doi.org/10.1039/C4NR05773B

177. Z. Hu, Q. Liu, S.-L. Chou, S.-X. Dou, Advances and challenges in metal sulfides/selenides for next-generation rechargeable sodium-ion batteries. Adv. Mater. **29**(48), 1700606 (2017). https://doi.org/10.1002/adma.201700606

178. J. Wang, C. Luo, T. Gao, A. Langrock, A.C. Mignerey, C. Wang, An advanced MoS$_2$/carbon anode for high-performance sodium-ion batteries. Small **11**, 473–481 (2015). https://doi.org/10.1002/smll.201401521

179. T. Lu, S. Dong, C. Zhang, L. Zhang, G. Cui, Fabrication of transition metal selenides and their applications in energy storage. Coord. Chem. Rev. **332**, 75–99 (2017). https://doi.org/10.1016/j.ccr.2016.11.005

180. Y. Chao, R. Jalili, Y. Ge, C. Wang, T. Zheng, K. Shu, G.G. Wallace, Self-assembly of flexible free-standing 3d porous MoS2-reduced graphene oxide structure for high-performance lithium-ion batteries. Adv. Funct. Mater. (2017). https://doi.org/10.1002/adfm.201700234

181. S. Byun, D.M. Sim, J. Yu, J.J. Yoo, High-power supercapacitive properties of graphene oxide hybrid films with highly conductive molybdenum disulfide nanosheets. ChemElectroChem **2**, 1938–1946 (2015). https://doi.org/10.1002/celc.201500393

182. X. Yang, S. Tang, G. Ding, X. Xie, M. Jiang, F. Huang, Layer-by-layer thinning of graphene by plasma irradiation and post-annealing. Nanotechnology **23**(2), 025704 (2012). https://doi.org/10.1088/0957-4484/23/2/025704

183. V. Nicolosi, M. Chhowalla, M.G. Kanatzidis, M.S. Strano, J.N. Coleman, Liquid exfoliation of layered materials. Science **340**(6139), 1420 (2013). https://doi.org/10.1126/science.1226419